CFD Simulation of Hydrodynamics of Three Phase Fluidized Bed

Thesis submitted

By

SHAILENDRA KUMAR PANDEY

(Roll. No - 208CH104)

In partial fulfillment for the award of the Degree of

Master of Technology

In

Chemical Engineering

Under the guidance of

Dr. H .M. JENA

Department of Chemical Engineering

National Institute of Technology

Rourkela-769008, Orissa India

May 2010

Dedicated to

Lordess Maa Durga

Department of Chemical Engineering

National Institute of Technology

Rourkela-769008, Orissa, India

CERTIFICATE

This is to certify that the thesis entitled, **"CFD Simulation of Hydrodynamics of Three Phase Fluidized Bed"** submitted by Shailendra Kumar Pandey (Roll. N0 - 208CH104) to National Institute of Technology, Rourkela in partial fulfillment of the requirements for the award of the degree Master of Technology in Chemical Engineering is an authentic work carried out by him under my supervision and guidance.

To the best of my knowledge, the matter embodied in the thesis has not been submitted to any other University/Institute for the award of any Degree/Diploma.

Dr. H. M. Jena
Department of Chemical Engineering
National Institute of Technology
Rourkela - 769008
INDIA

ACKNOWLEDGEMENT

In pursuit of this academic endeavor, I feel that I have been singularly fortunate; inspiration, guidance, direction, cooperation, love and care all came in my way in abundance and it seems almost an impossible task for me to acknowledge the same in adequate terms. Yes, I shall be failing in my duty if I do not record my profound sense of indebtedness and heartfelt gratitude to my supervisor ***Dr. H. M. Jena*** *who guided and inspired me in pursuance of this work. His association will remain a beacon light to me throughout my career.*

I am also thankful to ***Prof. G. K. Roy*** *for his valuable suggestion and support throughout last two year. I owe a depth of gratitude to* ***Prof. S. K. Agarwal****, H.O.D Department of Chemical Engineering.*

I am thankful to ***Prof. (Mrs.) Abanti sahoo*** *for acting as project coordinator and her support. I would like to thank the entire faculty of Chemical Engineering Department for their constant support throughout my course work. I want to acknowledge the support of all staff members and friends of Chemical Engineering, NIT Rourkela.*

I thank to the support, encouragement and best wishes of my parents and family members, without which I would have not been able to complete my thesis.

(Shailendra Kumar Pandey)

Abstract

The gas-liquid-solid fluidized bed has emerged in recent years as one of the most promising devices for three-phase operation. Such a device is of considerable industrial importance as evident from its wide application in chemical, refining, petrochemical, biochemical processing, pharmaceutical and food industries. Selection and design is one of the main parameter in the performance of three phase system. Success is dependent on the effective contact between the phases. Even though a large number of experimental studies have been done in different process parameters and physical properties, the complex hydrodynamics of three phase fluidized bed reactors are not well understood due to complicated phenomena such as particle–particle, liquid–particle and particle–bubble interactions. For this reason, computational fluid dynamics (CFD) has been promoted as a useful tool for understanding multiphase reactors for precise design and scale up. In the present work three different configuration of cylindrical column has been taken for studying co-current gas-liquid-solid fluidization with the help of commercial CFD codes as FLUENT 6.2. The main focus for analyzing the results is on the column with 1.88 m height and diameter of 0.1 m containing solid particles as glass beads of size 2.18 mm and 4.05 mm. In the present study of three phase fluidized simulation the hydrodynamic parameters investigated includes phase hold up, velocity profiles of all phases, bed expansion, bed voidage, static pressure drop, frictional pressure drop at wall, and energy flows. The operating variables varied includes liquid and air inlet velocity, initial solid static bed height and particle size. The dynamic characteristics obtained from CFD simulation have been validated with the experimental results and a good agreement has been observed. Eulerian-Eulerian granular multiphase flow approach is capable of predicting the overall performance of gas–liquid–solid fluidized bed. The expanded bed height is strong function of liquid velocity, it increases with liquid velocity. Velocity of the phases has been observed more in center region than near at wall in fluidized bed. Bed voidage increases with the liquid velocity and depending on the particle size. Axial velocity in small diameter column is more than the large diameter column. Frictional pressure drop at wall has been found to decrease with increase in the bed height.

Keywords: Fluidization, three-phase fluidized bed, bed expansion, computational fluid dynamics, Eulerian-Eulerian approach.

CONTENTS

List of figures

Figure No	Caption	Page
Fig. 5.6.	Velocity profiles of air with different bed height along radial direction in 1.88 m height fluidized bed at [V_l = 0.10616 m/s, V_g = 0.08 m/s, H_s = 0.213 m, D_p = 2.18 mm].	42
Fig. 5.7.	Plot of velocity magnitude of water at bed height of 0.35 m versus flow time in 1.88 m height fluidized bed at [V_l = 0.08 m/s, V_g = 0.09 m/s, H_s = 0.213 m, D_p = 2.18 mm].	43
Fig. 5.8.	Plot of velocity magnitude of solid glass beads at height of 0.35 m versus flow time in 1.88 m height fluidized bed at [V_l = 0.08 m/s, V_g = 0.09 m/s, H_s = 0.213 m, D_p = 2.18 mm].	44
Fig. 5.9.	Comparison of gas, solid and liquid velocities in 1.88 m height fluidized bed at [V_l = 0.09 m/s, V_g = 0.02123 m/s, H_s = 0.267 m, D_p = 4.05 mm].	44
Fig. 5.10.	Comparison of experimental work (Kiared et al., 1999) with simulation for axial solid velocity in 1.5 m height fluidized bed at [V_l = 0.065 m/s, V_g = 0.069 m/s, H_s = 0.35 m, D_p = 3 mm].	45
Fig. 5.11.	Axial velocity of solid with radial direction in 1.88 m height fluidized bed at [V_l = 0.04 m/s, V_g = 0.02123 m/s, H_s = 0.267 m, D_p = 4.05 mm].	46
Fig. 5.12.	Axial velocity of liquid with radial direction in 1.88 m height fluidized bed at [V_l = 0.04 m/s, V_g = 0.02123 m/s, H_s = 0.267 m, D_p = 4.05 mm].	47
Fig. 5.13.	Axial velocity of air with radial direction in 1.88 m height fluidized bed at [V_l = 0.04 m/s, V_g = 0.02123 m/s, H_s = 0.267 m, D_p = 4.05 mm].	47
Fig. 5.14.	Variation of solid velocity for different particles in 1.88 m height fluidized bed with the inlet liquid velocity at [V_g = 0.02123 m/s, H_s = 0.267 m].	48

Figure No	Caption	Page
Fig. 5.15.	Axial solid velocity profiles with radial direction for 0.1 m diameter fluidized bed at [V_l = 0.09 m/s, V_g = 0.02123 m/s, H_s = 0.267 m, D_p = 4.05 mm].	49
Fig. 5.16	Axial solid velocity profiles with radial direction for 0.254 m diameter column at [V_l = 0.09 m/s, V_g = 0.02123 m/s, H_s =0.267 m, D_p = 4.05 mm].	50
Fig. 5.17.	Comparison of average solid velocity in two different cylinders with bed height at [V_l = 0.09 m/s, V_g = 0.02123 m/s, H_s = 0.267 m, D_p = 4.05 mm].	50
Fig. 5.18.	Comparison of axial solid velocity in two different cylinders with bed height at [V_l = 0.09 m/s, V_g = 0.02123 m/s, H_s = 0.267 m, D_p = 4.05 mm].	51
Fig. 5.19	Radial solid velocity variation with time step in 1.88 m height column at [V_l = 0.09 m/s, V_g = 0.02548 m/s, H_s = 0.213 m, D_p = 2.18 mm].	51
Fig. 5.20.	Bed expansion of glass bead in 1.88 m height column at [V_l = 0.0637 m/s, V_g = 0.05096 m/s, H_s = 0.213 m, D_p = 2.18 mm].	52
Fig. 5.21.	Bed height variation with inlet liquid velocity at constant gas inlet velocity for 1.88 m height fluidized bed at [H_s = 0.213 m, D_p = 2.18 mm].	52
Fig. 5.22.	Comparison of bed expansion ratio of two different glass beads with experiment in 1.88 m height column at [V_g = 0.02123 m/s, H_s = 0.267 m].	53
Fig. 5.23.	Gas hold up variation with inlet liquid velocity for 1.88 m height column at [V_g = 0.02123 m/s, H_s = 0.267 m, D_p = 4.05 mm.].	54

List of Tables

List of Symbols

A	cell surface area, m^2
D	diameter of the column, m
D_p	diameter of solid glass beads, mm
d_p	diameter of the bubbles or droplets of phase p, m
E_D	energy dissipation by the liquid phase, W
E_e	energy dissipation rate due to turbulence in liquid phase, W
E_i	input energy due to liquid phase, W
E_{kg}	gas phase kinetic energy, W
E_{kl}	liquid phase kinetic energy, W
E_{out}	energy leaving the fluidized bed by liquid and gas phase, W
E_{Pg}	gas phase potential energy, W
E_{kS}	solid phase kinetic energy, W
E_{Pl}	potential energy of liquid leaving the fluidized bed, W
E_{Bls}	energy dissipated due to friction at liquid solid interface,w
E_{Blg}	energy dissipated due to friction at gas liquid interface,w
E_T	energy gained by solid phase, w
F	vector of fluxes
f	drag function
g	acceleration due to gravity, m/s^2
$G(\varepsilon_s)$	solid elastic modulus
G_0	reference elasticity modulus
G_κ	generation of turbulence kinetic energy due to the mean velocity gradients
G_b	generation of turbulence kinetic energy due to buoyancy
H	expanded bed height, m
H_s	static bed height of solid, m
κ	turbulence kinetic energy, m^2/sec^2

K_{sl}	drag factor of phase s in liquid phase, kg/m^{3}s
$M_{i,l}$, $M_{i,g}$, $M_{i,s}$	interphase force term for liquid, gas, and solid
P_s	solid pressure, kg/m s^2
Q	vector of conserved variables
R_e	relative Reynolds number
$\overline{u_g}$	local gas phase velocity vector, m/s
$\overline{u_l}$	local liquid phase velocity vector, m/s
$\overline{u_s}$	local solid phase velocity vector, m/s
V	cell volume, m^3
V_l , V_g	superficial velocityof liquid and gas, m/sec
v_s	time averaged solid velocity, m/s
V_{bs}	slip velocity between gas and liquid phase, m

Greek Symbols

α_l	liquid phase volume fraction
ε	turbulence dissipation rate
ε_l , ε_g , ε_s	volume fraction of liquid, gas and solid
ε_{sm}	maximum solid packing parameter
ρ_k	density of phase k = gas, solid, liquid, kg/ m3
μ_g , μ_l, μ_s	gas viscosity of gas, liquid and solid, kg/ms^2
μ_{tg}, μ_{ts}	induced turbulence viscosity gas and solid, kg/ms^2
$\mu_{T,l}$	liquid phase turbulent viscosity, kg/ms^2
σ_κ	turbulent Prandtl numbers for turbulence kinetic energy
σ_ε	turbulent Prandtl numbers for dissipation rate
$\mu_{eff,l}$	liquid phase effective viscosity, kg/ms^2
τ_p	particulate relaxation time, s

Chapter 1
Introduction

A fluid is anybody whose parts yield to any force impressed on it, and by yielding, are easily moved among themselves

Isaac Newton, from section V

Book of the principia, 1687

Chapter–1

Introduction

Fluidization is an operation through which fine solids are transformed into a fluid like state through contact with either a gas, liquid or both. Under the fluidized state, the gravitational pull on granular solid particles is offset by the fluid drag on them, thus the particles remain in a semi-suspended condition. At the critical value of fluid velocity the upward drag forces exerted by the fluid on the solid particles become exactly equal the downward gravitational forces, causing the particles to become suspended within the fluid. At this critical value, the bed is said to be fluidized and exhibit fluidic behavior.

In the 1920s, a fluidized bed gas generator was developed by Fritz Winkler in Germany which represented the first large-scale, commercially significant use of the fluidized bed (Kunii and Levenspiel., 1991). The fluidized bed reactor was first introduced into the petroleum industry through the fluid catalytic cracking (FCC) process by the Standard Oil Company of New Jersey (now ExxonMobil) in 1942. Here catalysts were used to reduce petroleum to simpler compounds through a process known as cracking. The invention of this technology made it possible to significantly increase the production of various fuels in the United States.

1.1. Three phase fluidized bed

The three phase fluidized bed is a type of system that can be used to carry out a variety of multiphase chemical reactions. In this type of reactor, gas and liquid are passed through a granular solid material at high enough velocities to suspend the solid in fluidized state. The solid particles in the fluidized bed are typically supported by a porous plate, known as a distributor at the static condition. The fluid is then forced through the distributor up through the solid material. At lower fluid velocities, the solids remain in place as the fluid passes through the voids in the material. As the fluid velocity is increased, the bed reaches a stage where the force of the fluid on the solids is enough to balance the weight of the solid material. This stage is known as incipient fluidization and the corresponding fluid velocity is called the minimum fluidization velocity. Once this minimum velocity is surpassed, the contents of the bed begin to expand and swirl around much like an agitated tank or boiling pot of water, the system is now a fluidized bed (Howard., 1989). Three-phase fluidized bed reactors are used extensively in chemical, petrochemical, refining, pharmaceutical, biotechnology, food and environmental industries. The most common occurrence of gas–liquid-solid phase systems is in hydro processing industry in which variety of reactions between hydrogen and oil phase with solid catalyst have been found. The other common three phase reactions are catalytic oxidation and hydration reactions. Three phase fluidization systems, the phase are reacting with different forms as:

- Reactions where the gas, liquid and solid are either reactants or products.
- Gas-Liquid reactions with solid as a catalyst.
- Two reaction phases and third as inert phase.
- All three phases are inert as found in unit operations.

Depending on the density and volume fraction of particles, three-phase reactors can be classified as slurry bubble column reactors and fluidized bed reactors. In slurry bubble column reactors, the density of the particles are slightly higher than the liquid and particle size is in the range of 5–150 μm and volume fraction of particles is below 0.15 hence, the liquid phase along with particles is treated as a homogenous liquid with mixture density. But in fluidized bed reactors, the density of particles are much higher than the density of the liquid and particle size is normally large (above 150 μm) and volume fraction of particles varies from 0.6 (packed stage) to 0.2 as close to dilute transport stage (Panneerselvam et al., 2009).

1.2. Advantages of three phase fluidized bed

The three phase fluidized beds are increasingly used as reactors as they overcome some inherent drawback of conventional reactors and add more advantages. Some of the advantages of three phase fluidized bed reactor are as follow (Trambouze and Euzen., 2004).

- High rate of reaction per unit reactor volume can be obtained through these reactors.
- The major advantages of these reactors are, they give high turbulence, better flexibility of mixing, heat recovery and temperature control.
- The better mixing and in these reactors prevents the formation of local hot spots.
- The three phase fluidized bed offers better gas phase distribution creating more gas-liquid interfacial area.

- Ability to continuously withdraw product and introduce new reactants into the reaction vessel allows production more efficiently due to the removal of startup conditions as in case of batch processes.
- They allow use of fine catalyst particles, which minimizes the intraparticle diffusion. Smaller is the particle larger is surface area which enables more intimate contact of phases and enhances the rector performance.
- These reactors can effectively be used for the rapidly deactivating catalyst and three phase reactions where solid is catalyst and also solid is used as reactant (e.g. catalytic coal liquefaction).
- Bubbling and circulating fluidized bed systems are becoming an increasingly important. in technology for the power generation, mineral and chemical processing industries.
- Benefits in economic, operational and environmental terms can be achieved with fluidized bed technology over more traditional technologies.

1.3. Application of Three phase fluidized bed

The gas-liquid-solid fluidized bed has emerged in recent years as one of the most promising devices for three-phase operation. Such a device is of considerable industrial importance as evident from its wide application in chemical, petrochemical and biochemical processing (Muroyama et al., 1985). Fluidized beds serve many purposes in industry, such as facilitating catalytic and non-catalytic reactions. Three-phase fluidized beds have been applied successfully to many industrial processes such as in the Hydrogen-oil process for hydrogenation and hydro-desulfurization of residual oil, the H-coal process for coal liquefaction, and Fischer–Tropsch process (Jena et al., 2009). Some more applications of fluidized bed are follow as:

- Turbulent contacting absorption for flue gas desulphurization.
- Bio-oxidation process for wastewater treatment.
- Physical operations such as drying and other forms of mass transfer.
- Biotechnological processes such as fermentation and aerobic wastewater treatment.
- Methanol production and conversion of glucose to ethanol.
- Pharmaceuticals and mineral industries.
- Oxidation of naphthalene to phathalic anhydride (catalytic).

- Coking of petroleum residues (non-catalytic).

1.4. Drawbacks of fluidized bed

As in any design, the fluidized bed reactor does have it draw-backs, which any reactor designer must take into consideration (Trambouze and Euzen, 2004).

- **Increased Vessel Size:** Because of the expansion of the bed materials in the reactor, a larger vessel is often required than that for a packed bed reactor. This larger vessel means that more must be spent on initial capital costs.
- **Pumping Requirements and Pressure Drop:** The requirement for the fluid to suspend the solid material necessitates that a higher fluid velocity is attained in the reactor. In order to achieve this, more pumping power and thus higher energy costs are needed. In addition, the pressure drop associated with deep beds also requires additional pumping power.
- **Particle Entrainment:** The high gas velocities present in this reactor often result in fine particles becoming entrained in the fluid. These captured particles are then carried out of the reactor with the fluid, where they must be separated. This can be a very difficult and expensive problem to address depending on the design and function of the reactor.
- **Erosion of Internal Components:** The fluid-like behavior of the fine solid particles within the bed eventually results in the wear of the reactor vessel. This can require expensive maintenance and upkeep for the reaction vessel and pipes.
- **Lack of Current Understanding:** Current understanding of the actual behavior of the materials in a fluidized bed is rather limited. It is very difficult to predict and calculate the complex mass and heat flows within the bed. Due to this lack of understanding, a pilot plant for new processes is required. Even with pilot plants, the scale-up can be very difficult and may not reflect what was experienced in the pilot trial.

1.5. Modes of operation of gas-liquid-solid fluidized bed and flow regimes

Based on the differences in flow directions of gas and liquid and in contacting patterns between the particles and the surrounding gas and liquid, several types of operation for gas-liquid-solid fluidizations are possible. Gas-liquid-solid fluidization can be classified mainly into four modes of operation. These modes are co-current three-phase fluidization with liquid as the continuous phase; co-current three-phase fluidization with gas as the continuous phase; inverse three-phase fluidization and fluidization by a turbulent contact absorber (TCA). Due to the complex nature of three-phase fluidization, however, various method are possible in evaluating the operating and design parameters for each mode of operation. Countercurrent bubble flow with liquid-supported solids which can be affected by downward liquid fluidization of particles having a density lower than that of the liquid has been referred to as inverse three-phase fluidization. The liquid-supported solids operation characterizes fluidization with the liquid velocity beyond the minimum fluidization velocity. The bubble-supported solids operation characterizes fluidization with the liquid velocity below the minimum fluidization velocity where the liquid may even be in a stationary state. Countercurrent three-phase fluidization with gas as the continuous phase is known as a turbulent contact absorber, fluidized packing absorber, mobile bed or turbulent bed contactor. (Epstein., 1981).

1.6. Variables affect the quality of fluidization

Some of the variables affecting the quality of fluidization are as follow:

- Fluid flow rate: It should be high enough to keep the solids in suspension but it should not be so high that the fluid channeling occurs.
- Fluid inlet: It must be designed in such a way that the fluid entering the bed is well distributed.
- Bed height: With other variables remaining constant, the greater the bed height, the more difficult it is to obtain good fluidization.
- Particle size: It is easier to maintain fluidization quality with particles having a wide range than with particles of uniform size.
- Gas, Liquid and solid densities: The closer the relative density of the gas, liquid and the solid, the easier is to maintain smooth fluidization.

1.7. Complexion of three phase system

Selection and design of reactors is one of the main parameter in the performance of three phase system. As three phase system is highly complex and the success of three phase system is essentially dependent on the effective contact of each phases with other. Even though a large number of experimental studies have been carried out for different process parameters and physical properties, the complex hydrodynamics of three phase fluidized bed reactors are not well understood due to complicated phenomena such as particle–particle, liquid–particle and particle–bubble interactions. For this reason, computational fluid dynamics (CFD) has been promoted as a useful tool for understanding multiphase reactors (dudukovic et al., 1999) for precise design and scale up. By using CFD various reactors and phase contactors were studied and operated successfully.

1.8. Present work

The present work is concentrated on understanding the complex hydrodynamics of three-phase fluidized beds. Three different fluidized bed system of height 1.88 m, 1.5 m and 2.5m with diameter of 0.1 m, 0.1 m and 0.254 m respectively have been simulated. The solid phase used is glass beads of size 2.18, 2.3, 3 and 4.05 mm in the present work. Co-current gas-liquid-solid fluidization with liquid as continuous phase has been used. The static bed heights of the solid phase in the fluidized bed used for simulation are taken as 21.3 cm, 26.7 cm, 35 cm and 39 cm respectively. Initial solid hold up has been taken as 0.59 in all cases with superficial velocity of gas varying in the range of 0.025 - 0.127 m/sec and that of the liquid ranges to 0.031-0.14 m/s. The CFD simulations have been carried out using commercial CFD software FLUENT 6.2. The aim is to simulate the three phase fluidized bed to find out the effect of various operating parameters on the hydrodynamics. The hydrodynamics parameters for investigation are bed expansion, holdup of all three phases, bed voidage, velocity profiles, static pressure and frictional pressure drop at wall. The energy flows calculation has also been carried out for obtaining the net energy difference which should account for energy dissipated in the system.

1.9 Thesis layout

The second chapter of thesis contains a detailed literature survey of experimental and computational work on three phase fluidization. In third chapter CFD modeling of three phase fluidized bed has been described in detail and various approaches applied in CFD modeling have been discussed. Detail descriptions of numerical techniques and methods for solving computational model have been discussed in fourth chapter. In the fifth chapter results obtained from CFD simulation have been presented and discussed. In the last chapter (Chapter - 6) conclusion have been drawn on present work and scope of the future work have been presented.

Chapter 2

Literature Review

Chapter–2

Literature Review

This chapter provides a literature survey on three phase fluidization process comprising of both experimental and computational work.

2.1. Experimental survey

A significant amount of experimental study on the hydrodynamic and other characteristic behavior of three phase fluidized bed has been carried out. Most of the previous studies related to three-phase fluidized bed reactors have been directed towards the understanding the complex hydrodynamics, and its influence on the phase holdup and transport properties. Recent research on fluidized bed reactors focuses on flow structure and flow regime identification is being discussed below:

- **Flow structure quantification** - The quantification of flow structure in three-phase fluidized beds mainly focuses on local and globally averaged phase holdups and phase velocities for different operating conditions and parameters. Rigby et al. (1970), Muroyama and Fan (1985), Lee and De Lasa (1987) investigated bubble phase holdup and velocity in three-phase fluidized beds for various operating conditions using experimental techniques like electroresistivity probe and optical fiber probe. Recently Warsito and Fan (2001, 2003) quantified the solid and gas holdup in three-phase fluidized bed using the electron capacitance tomography (ECT) (Panneerselvam., 2009).

- **Flow regime identification** - Muroyama and Fan (1985) developed the flow regime diagram for air–water–particle fluidized bed for a range of gas and liquid superficial velocities. Chen et al. (1995) investigated the identification of flow regimes by using pressure fluctuations measurements. Briens and Ellis (2005) used spectral analysis of the pressure fluctuation for identifying the flow regime transition from dispersed to coalesced bubbling flow regime based on various data mining methods like fractal and chaos analysis, discrete wake decomposition method etc. Fraguío et al. (2006) used solid phase tracer experiments for flow regime identification in three phase fluidized beds (Panneerselvam., 2009).

Some of the various investigations done by researchers on three phase fluidization are mentioned below:

- Wen Y. Soung (1978) has determined bed expansion data for three-phase fluidization for beds of commercial Co-Mo catalysts in n-heptane and nitrogen in Lucite tubes diameter. Gas and liquid velocities have been varied .Three cylindrical catalysts sizes, with same length but different in diameter have been used. Contraction of the bed due to gas injection has been observed with 0.1270 cm particles. This phenomenon is much less perceptible and no contraction at all with gas injection has been observed in a bed of 0.1600 cm catalyst. An attempt has been made to isolate the gas injection effect on bed expansion from the effect of liquid velocity. A correlation has been developed for the effect of gas velocity on bed expansion, based on particle Reynolds number, sphericity of the particle, and the liquid-to-gas velocity ratio. The result shows that the catalyst bed will expand substantially upon gas injection if the liquid-to-gas velocity ratio is kept below a certain value.

- Fan et al. (1982) have worked on the hydrodynamic behavior of inverse fluidization in the liquid-solid and gas-liquid-solid systems. In the liquid-solid system, particles fluidized with the downward flow of water and six different particles made of polyethylene or polypropylene have been utilized in this study. In the gas-liquid-solid system, air has been introduced into the bed counter currently to the water flow. An extensive investigation has been done for flow regime diagram of inverse gas-liquid-solid fluidization. The bed porosity and gas holdup have been obtained empirically and correlated.

- Yu and Kim (1988) have investigated the bubble characteristics in the radial direction of three phase fluidized bed with four different particle size ranges 0.4 – 0.6 mm. In this study the bubble hold up and mean velocity have been determined by means of u shaped optical fiber probe made of plastic. They have found that the liquid velocity did not significantly affect the bubble rising velocity.

- Krishnaiah et al. (1993) have conducted experiments to study the hydrodynamics of three phase inverse fluidized beds using very light particles. The experimental data for the minimum liquid velocity at the onset of fluidization has been correlated in terms of the physical properties of the fluids, particle characteristics and system variables. Correlations for the friction factor have also been proposed.

- Comte et al. (1997) have studied on the hydrodynamics of a three-phase inverse turbulent bed. A detailed idea about critical gas velocities like the gas velocity required to distribute the particles over the whole height of the reactor and gas velocity required for a uniform axial distribution of the solids have been discussed.

- Kiared et al. (1999) have investigated the solid phase hydrodynamics in three-phase fluidized bed using radioactive particle tracking. Experimental descriptions of the time-averaged solids flow in the fully developed region of a cylindrical gas-liquid-solid fluidized bed have been provided by using a non invasive radioactive particle tracking technique (RPT). The 3-D local instantaneous velocity components (radial, axial, azimuthal) of a single radioactive solid tracer have been measured over extended time period. Radial distributions of axial and radial mean turbulent velocities of particle, shear stress and eddy diffusion coefficients have been established.

- Sokol and Halfani (1999) have studied the hydrodynamics of gas-liquid-solid fluidized bed bioreactor with a low density biomass support (matrix density smaller than that of water) .It has been found that the air hold up increases with increase in the inlet air velocity.

- Allia et al. (2006) have carried out the hydrodynamic study of three phase fluidized bed bioreactors used for the removal of hydrocarbons from the refinery waste water. The study allowed the determination of operating conditions before treatment experiments. The obtained results have shown that in the three-phase fluidized bed the hydrocarbons degrade more rapidly than in a closed aerated bioreactor.

Even though a large number of experimental studies have been directed towards the quantification of flow structure and flow regime identification for different process parameters and physical properties, the complex hydrodynamics of these reactors are not well understood due to the interaction of all the three phases simultaneously. It has been a very tedious task to analyze the hydrodynamic property in experimental way of three phase fluidized bed reactor, so another advanced modeling approaches based on CFD techniques have been applied for investigation of three phases for accurate design and scale up. Basically two approaches namely, the Euler–Euler formulation based on the interpenetrating multi-fluid model, and the Euler–Lagrangian approach based on solving Newton's equation of motion for the dispersed phase are used.

2.2. Survey on CFD modeling

- Bahary et al. (1994) have used Eulerian multi-fluid approach for three-phase fluidized bed, where gas phase treated as a particulate phase having 4 mm diameter and a kinetic theory granular flow model applied for solid phase. They have simulated both symmetric and axisymmetric model and verified the different flow regimes in the fluidized bed by comparing with experimental data.

- Grevskott et al. (1996) have used Eulerian–Eulerian model approaches for three-phase bubble column. The liquid phase along with the particles has been considered pseudo-homogeneous by modifying the viscosity and density. The bubble size distribution based on the bubble induced turbulent length and the local turbulent kinetic energy has been studied. Variations of bubble size distribution, liquid circulation and solid movement along radial direction have been discussed.

- Mitra-Majumdar et al. (1997) have taken multi-fluid Eulerian approach for three-phase bubble column. They have used modified drag correlation between the liquid and the gas phase to account for the effect of solid particles and between the solid and the liquid phase to account for the effect of gas bubbles. A k–ε turbulence model has been used for the turbulence and considered the effect of bubbles on liquid phase turbulence. Axial variation of gas holdup and solid holdup profiles for various range of liquid and gas superficial velocities and solid circulation velocity have been examined.

- Jianping and Shonglin (1998) have worked in 2-D with Eulerian–Eulerian method for three-phase bubble column for turbulence. $k_{sus}-\varepsilon_{sus}-k_b-\varepsilon_b$ turbulence model and Pseudo-two-phase fluid dynamic model have been used. The local axial liquid velocity and local gas holdup with have been validated experimental data.

- Li et al. (1999) have studied in 2-D with Eulerian–Lagrangian model for three-phase fluidization. The Eularian fluid dynamic method, the dispersed particle method (DPM) and the volume-of-fluid (VOF) method have been used to account for the flow of liquid, solid and gas phases respectively. A continuum surface force (CSF) model, a surface tension force model and Newton's third law have been applied to account for the interphase couplings of gas–liquid, particle–bubble and particle–liquid interactions respectively. A close distance interaction (CDI) model included in the particle–particle collision analysis, which considers the liquid interstitial effects between colliding particles. Single bubble rising velocity in a liquid–solid fluidized bed and the bubble wake structure and bubble rise velocity in liquid and liquid–solid medium have been investigated.

- Padial et al. (2000) have worked in 3-D with multi-fluid Eulerian approach for three-phase draft-tube bubble column. The drag force between solid particles and gas bubbles has been modeled in the same way as that of drag force between liquid and gas bubbles. The gas volume fraction and liquid circulation in draft tube bubble column have been simulated.

- Joshi et al. (2001) have studied the bubble column reactors using Computational flow modeling with Euler–Lagrange approach. Understanding of the drag force, virtual mass force and lift force and mechanism of the energy transfer from gas to liquid phase have been explained. By using phases flow pattern results the effort has been concentrated to design cylindrical bubble column. The effects of the superficial gas velocity, column diameter and bubble slip velocity on the flow pattern have been examined and compared with experimental velocity profiles.

- Joshi et al. (2002) have determined the prediction of flow pattern near the wall and pressure drop in a bubble column reactor using k–ε based model with low Reynolds number. Specific attention has been given to the modeling of momentum transfer near the wall. An excellent agreement has been shown between the predicted and experimental hold-up and velocity profiles over a wide range of superficial gas velocity, column diameter, column height and the nature of gas–liquid system (bubble diameter and their rise velocity).

- Matonis et al. (2002) have worked in 3-D with multi-fluid Eulerian approach for slurry bubble column and used the Kinetic theory granular flow (KTGF) model for describing the particulate phase. The k–ε based turbulence model has been taken for liquid phase turbulence and the analysis of the time averaged solid velocity, volume fraction profiles, shear Reynolds stress have been done and compared with experimental data.

- Feng et al. (2005) have used 3-D, multi-fluid Eulerian approach for three-phase bubble column. The liquid phase along with the solid phase considered as a pseudo-homogeneous phase in view of the ultrafine nanoparticles. The interface force model of drag, lift and virtual mass and k–ε model for turbulence have been taken. They compared the local time averaged liquid velocity and gas holdup profiles along the radial position.

- Schallenberg et al. (2005) have used 3-D, multi-fluid Eulerian approach for three-phase bubble column. Gas–liquid drag coefficient based on single bubble rise modified for the effect of solid phase. Extended k–ε turbulence model to account for bubble-induced turbulence has been used and the interphase momentum between two dispersed phases included. Local gas and solid holdup as well as liquid velocities have been validated with experimental data.

- Zhang and Ahmadi (2005) have used 2-D, Eulerian–Lagrangian model for three-phase slurry reactor where interactions between bubble–liquid and particle–liquid have been included. Particle–particle and bubble–bubble interactions have been accounted for by the hard sphere model approach. Bubble coalescence has also been included in the model. Transient characteristics of gas, liquid, and particle phase flows in terms of flow structure, effect of bubble size on variation of flow patterns and instantaneous velocities have been studied.

- Panneerselvam et al. (2009) have worked in 3D, Eulerian multifluid approach for gas-liquid-solid fluidized bed. Kinetic theory granular flow (KTGF) model for describing the particulate phase and a k-ε based turbulence model for liquid phase turbulence have been used. The interphase momentum between two dispersed phases has been included. Radial distributions of axial and radial solid velocities, axial and radial solid turbulent velocities, shear stress, axial bubble velocity, axial liquid velocity and averaged gas holdup and various energy flows have been studied.

- O'Rourke et al. (2009) have used 3D, Eulerian finite difference approach for gas-liquid-solid fluidized bed. The mathematical model using multiphase particle-in-cell (MP-PIC) method has been used for calculating particle dynamics (collisional exchange) in the Computational-particle fluid dynamics (CPFD). Mass averaged velocity of solid and liquid, particle velocity fluctuation, collision time, and liquid droplet distribution have been studied.

Chapter 3

CFD Modeling Of Three Phase Fluidized bed

All the mathematical sciences are founded on
Relations between physical laws and laws of
numbers, so that the aim of exact science is to
reduce the problems of nature to the determination
of quantities by operations with numbers.

James Clerk Maxwell, 1856

Chapter–3

CFD Modeling Of Three Phase Fluidized bed

3.1. Computational fluid dynamics (CFD)

CFD is the science of predicting fluid flow, heat transfer, mass transfer, chemical reactions, and related phenomena by solving the mathematical equations which govern these processes using a numerical process. By means of computer based simulation.CFD is one of the branches of fluid mechanics that uses numerical methods and algorithms to solve and analyze problems that involve fluid flows (Bakker., 2002). Computers are used to perform the millions of calculations required to simulate the interaction of fluids and gases with the complex surfaces used in engineering. However, even with simplified equations and high speed supercomputers, only approximate solutions can be achieved in many cases. More accurate codes that can accurately and quickly simulate even complex scenarios such as supersonic or turbulent flows are an ongoing area of research. The fundamental basis of any CFD problem is the Navier-Stokes equations, which define any single-phase fluid flow. These equations can be simplified by removing terms describing viscosity to yield the Euler equations. Further simplification, by removing terms describing vorticity yields the full Potential equations. CFD uses numerical methods to solve these fundamental nonlinear differential equations for pre-defined geometries and boundary conditions to linearized form. The result is a wealth of predictions for flow velocity, temperature, and phase hold up, pressure etc for any regions where flow occurs. The result of CFD analysis is relevant engineering data which are used in conceptual studies of new designs, detailed product development, troubleshooting, and design. (Anderson, 1995). The various general-purpose CFD packages in use are PHONICS, CFX, FLUENT, FLOW3D and STAR-CD etc. Most of these packages are based on the finite volume method and are used to solve fluid flow and heat and mass transfer problems.

3.2. Advantages of CFD

Over the past few decades, CFD has been used to improve process design by allowing engineers to simulate the performance of alternative configurations, eliminating guesswork that would normally be used to establish equipment geometry and process conditions. The use of CFD enables engineers to obtain solutions for problems with complex geometry and boundary conditions. CFD is very attractive to industry and research since it has many advantages as follows (Park., 2009).

- **Cost-effective** - CFD is relatively low cost than the physical testing Using physical experiments and tests to get essential engineering data for design can be expensive. CFD simulations are relatively inexpensive, and costs are likely to decrease as computers become more powerful.
- **Speed** - CFD simulations can be executed in a short period of time. Engineers can evaluate the performance of wide range system configuration on the computer without the time expense.
- **Flexibility** - It provides the flexibility to change design parameters without changing actual System changes, thus allowing engineers to try more alternative designs than would be feasible otherwise.
- **Ability to simulate real conditions** - Many flow and heat transfer processes cannot be (easily) tested, e.g. hypersonic flow and process operating at high temperature and pressure. CFD provides the ability to theoretically simulate any physical condition.
- **Wide information** - CFD allows the analyst to examine a large number of locations in the region of interest. Experiments only permit data to be extracted at a limited number of locations in the system.
- **CFD is reliable -** The results obtain from CFD analysis are very much validating with experiments also numerical schemes and methods upon which CFD is based are improving rapidly, so CFD results are increasingly reliable.

3.3. Application of CFD

CFD is useful in a wide variety of Industrial and non-industrial application areas. Currently, its main application is as an engineering method to provide data, which suits to solving the real problem of the physical world. Applications of CFD are numerous and diversified, some of which are given below (Bakker., 2002).

- In Chemical process industry, CFD is most helpful for equipment designers to help analyze and design the flow and performance of process industry equipment such as, Stirred tank, Fluidized bed reactor, Separators, Combustion systems, Heat exchangers, polymer and material processing and handling equipment.
- Designing of Aerodynamics of ground vehicles, aircraft and missiles for efficient

performance CFD is used.

- Bio-medical engineering is a rapidly growing field and uses CFD to study the circulatory and respiratory systems and blood flow through arteries and veins.
- Flow and heat transfer in power generation systems (boilers, combustion equipment, pumps, blowers, piping, etc.).
- CFD is related to architectural applications like indoor air simulation, outdoor air simulation (i.e. around the building), environmental suitability, Ventilation, heating, cooling flows in buildings and wind loading.
- CFD has found its application with semiconductor industry in cooling of equipment including micro-circuits. CFD solution can help immensely in reducing the number of experiments required to design various chip manufacturing equipments. Various semiconductor industries have started using CFD calculation to help their design engineers.
- In steel Industry it is being used in a big way to optimize the processes. High temperature and visual opacity of the liquid steel makes it difficult to carry out, so CFD has been useful to visualize the flow of steel in the industrial vessels and improve its performance.
- CFD are used in designing related to turbo machinery applications like diffusers, compressors and turbines.
- CFD has a long tradition in glass industry. The measurement of flow quantities is very difficult and therefore simulation greatly helps to understand, evaluate and optimize all applicable processing steps.
- It is also applied in Marine engineering and oceanography study.

3.4. Limitations of CFD

In spite of large advantages and applications of CFD, it has some few limitations which are as follows (Bakker., 2002).

Physical models - CFD solutions rely upon physical models of real world processes (e.g. turbulence, compressibility, chemistry, multiphase flow, etc.).The CFD solutions can only be as accurate as the physical models on which they are based.

Numerical errors - Solving equations on a computer invariably introduces numerical errors.

Round-off error is due to finite word size available on the computer. Round-off errors will always exist (though they can be small in most cases).Second error which found in CFD simulations is truncation error, due to approximations in the numerical models.

Boundary conditions - As with physical models, the accuracy of the CFD solution is only as good as the initial/boundary conditions provided to the numerical model.

3.5. Working of CFD code

In order to provide easy access to their solving power all commercial CFD packages include sophisticated user interfaces input problem parameters and to examine the results. Hence all codes contain three main elements (Bakker., 2002).

1. Pre-processing
2. Solver
3. Post –processing.

3.5.1. Pre-Processing

In Preprocessing, it consist of input of a flow problem by means of an operator friendly Interface and subsequent transformation of this input into a suitable form which can be used by the solver. This step is performed by software tool such as, GAMBIT, TGRID and DM (Design modular of ANSYS) .The Pre-processing stage involves the following steps (Bakker., 2002).

- Defining the geometry of the region for computational domain.
- Generating the Grids for subdivision of the domain into a number of smaller, non-overlapping sub domains.
- Specifying the appropriate boundary and continuum conditions at cells, which coincide with or touch the boundary.

The solution of a flow problem (Phase hold up, velocity, pressure, temperature etc.) is defined in each cell in various non linear equations form. The accuracy of CFD solutions is governed by number of cells in the grid. In general, the larger numbers of cells better the solution accuracy.

3.5.2. Solver

The CFD solver does the flow calculations and produces the desired results. FLUENT uses the finite-volume method to solve the governing equations for a fluid. It provides the capability to use different physical models such as incompressible or compressible, inviscid or viscous, laminar or turbulent, etc. Governing equations are non-linear and coupled, several iterations of the solution loop are performed by solver before a converged solution is obtained (Bakker., 2002) and the main functions of Solver are as follows:

- Approximation of unknown flow variables by means of simple functions.
- Discretization by substitution of the approximation into the governing flow equations and subsequent mathematical manipulations.
- Solving the algebraic equations.

3.5.3. Post-Processing

This is the final step in CFD analysis, and it involves the results and interpretation of the predicted flow data. FLUENT software includes full post processing capabilities and exports CFD data to third-party post-processors and visualization tools such as Ensight, Fieldview and TechPlot (Bakker., 2002).The main outcomes of post processing are -

- Domain geometry & Grid display.
- Contour plot of all the properties.
- Vector plots.
- Animations.
- 2D & 3D surface plots.
- X-Y plots with different properties.
- Particle tracking.
- Plot convergence.
- View manipulation (translation, rotation, scaling etc.).

3.6. Approaches to multiphase modeling

With the advent of increased computational capabilities, computational fluid dynamics, is emerging as a very promising new tool in modeling hydrodynamics. While it is now a standard tool for single-phase flows, it is at the development stage for multiphase systems, such as fluidized beds. Work is required to make CFD suitable for fluidized bed reactor modeling and scale-up purposes. The fundamental problem encountered in modeling hydrodynamics of fluidized bed is the motion of the multiphase of which the interface is unknown, transient, and the interaction is understood only for a limited range of conditions (Muthu et al., 2008). The first intuition in resolving the multiphase mixture is to treat each phase by standard continuum mechanics with boundary and jump conditions to solve the governing equations at the interfaces (Gamwo et al., 1998). However, it is quickly realized that the mathematical complexities of the non-linearity of the equations and in defining the interpenetrating and moving phase boundaries make numerical solutions very difficult. When multiple fluids are involved in a flow field, representing them by multiple species equations only works if the fluids are mixing and not separating. Any separation caused by the action of body forces, such as gravity or centrifugal force, can only be captured by treating the fluids with a multiphase model. When such a model is used, each of the fluids is assigned a separate set of properties, including density. Because different densities are used, forces of different magnitude can act on the fluids, enabling the prediction of separation (Muthu et al.,2008). Two different approaches have been applied in early attempts to apply CFD modeling to gas-liquid-solid fluidized bed.

1. Euler-Lagrange approach
2. Euler-Euler approach

3.6.1. The Euler-Lagrange approach

The Lagrangian discrete phases model in FLUENT follows the Euler-Lagrange approach. The fluid phase is treated as a continuum by solving the time-averaged Navier-Stokes equations, while the dispersed phase is solved by tracking a large number of particles, bubbles, or droplets through the calculated flow field. The dispersed phase can exchange momentum, mass, and energy with the fluid phase. A fundamental assumption made in this model that the dispersed second phase occupies a low volume fraction, even though high mass loading i.e. mass load of particle is greater than the mass load of fluid, is acceptable. The particle or droplet trajectories are computed individually at specified intervals during the fluid phase calculation. This makes the model appropriate for the modeling of spray dryers, coal and liquid fuel combustion, and some particle-laden flows, but inappropriate for the modeling of liquid-liquid mixtures, fluidized beds or any application where the volume fraction of the second phase is not negligible. Due to computational limitations, the Euler-Lagrangian model is normally limited to a number of particles of order 10^6. For small particles, such as typical catalyst particle diameters of 75 μm, it becomes difficult to simulate any meaningful reactor volume. Eulerian Lagrangian approach is easy to model, but it is difficult to program (Muthu et al., 2008).

3.6.2. The Euler-Euler Approach

In the Euler-Euler approach, the different phases are treated mathematically as interpenetrating continua. Since the volume of a phase cannot be occupied by the other phases, the concept of volume fraction is introduced. These volume fractions are assumed to be continuous functions of space and time and their sum is equal to one. Conservation equations for each phase are derived to obtain a set of equations, which have similar structure for all phases. These equations are closed by providing constitutive relations that are obtained from empirical information, or, in the case of granular flows, by application of kinetic theory. Euler-Euler approach are relatively faster but requires proper formulation of the constitutive equations. In FLUENT, three different Euler-Euler multiphase models are available: the volume of fluid (VOF) model, the mixture model, and the Eulerian model.

3.6.2.1. The VOF Model

The VOF model can model two or more immiscible fluids by solving a single set of momentum equations and tracking the volume fraction of each of the fluids throughout the domain. Because the fluids do not mix, each computational cell is filled with purely one fluid and purely another fluid or the interface between two (or more) fluids. Because of this unique set of conditions, only a single set of Navier-Stokes equations is required. Each fluid is allowed to have a separate set of properties. The properties used are those of the fluid filling the control volume. If the interface lies inside the control volume, special treatment is used to track its position and slope in both the control volume and neighboring cells as the calculation progresses. This model is used to track free surface flows or the rise of large bubbles in a liquid, prediction of jet breakup, the motion of large bubbles in a liquid, the motion of liquid after a dam break, the steady or transient tracking of any liquid-gas interface stratified flows, filling and sloshing (Bakker., 2002).

3.6.2.2. The Mixture Model

The mixture model is designed for two or more phases (fluid or particulate). As in the Eulerian model, the phases are treated as interpenetrating continua. The mixture model solves for the mixture momentum equation and prescribes relative velocities to describe the dispersed phases. Applications of the mixture model include particle-laden flows with low loading, bubbly flows, sedimentation, and cyclone separators. The mixture model can also be used without relative velocities for the dispersed phases to model homogeneous multiphase flow.

3.6.2.3. The Eulerian Model

The Eulerian model is the most complex of the multiphase models in FLUENT. It solves a set of n momentum and continuity equations for each phase. Coupling is achieved through the pressure and interphase exchange coefficients. The manner in which this coupling is handled depends upon the type of phases involved; granular (fluid-solid) flows are handled differently than non-granular (fluid-fluid) flows. For granular flows, the properties are obtained from application of kinetic theory. Momentum exchange between the phases is also dependent upon the type of mixture being modeled. FLUENT's user-defined functions allow customizing the calculation of the momentum exchange. In Eularian multi-fluid model the treating of fluid and solid phases as interpenetrating continuum phases. The solid particles in such multi-fluid models are generally considered to be identical having a representative diameter and density. The general idea in formulating the multi-fluid model is to treat each phase as an interpenetrating continuum and therefore to construct integral balances of continuity, momentum and energy for all phases, with appropriate boundary conditions and jump conditions for phase interfaces. Since the resultant continuum approximation for the solid phase has no equation of state, and lacks some variables such as viscosity and normal stress (Pain et al., 2001). Certain averaging techniques and assumptions must be made to obtain a momentum balance for the solids phase. Applications of the Eulerian multiphase model include bubble columns, risers, particle suspension and fluidized beds.

3.7. Guidelines for multiphase models

In general, the best representation for a multiphase system can be selected by using appropriate model based on following guidelines.

- In bubble, droplet and particle-laden flows in which dispersed-phase volume fractions are less than or equal to 10% the discrete phase model is used.

- In bubble, droplet and particle-laden flows in which phase mixture or dispersed phase volume fractions exceed 10%, the mixture model is used.
- VOF model is used in case of Slug flow, stratified or free-surface flow.
- In pneumatic transport mixture model for homogenous flow or the Eulerian Model for granular flow is used.
- Eulerian model for granular flow is used for fluidized bed.
- In slurry flows and hydro transport, Eulerian or Mixture model is used.
- In sedimentation, Eulerian Model is used.

In present work Eulerian Model for granular flow has been used for modeling three phase fluidized bed reactor .This model capture fluidization phenomena in fluidized bed better than other available models The result predicted by this model is promising in most cases, so it is reliable to choose this one.

3.8. Computational flow model

All of CFD in one form or another is based on the fundamental governing equations of fluid dynamics i.e the continuity, momentum and energy conservation equations. These are the mathematical statements of three fundamental physical principles upon which all of fluid dynamics is based.

1. Mass is conserved.
2. Newton's second law.
3. Energy is conserved.

A solid body is rather easy to see and define but on the other hand, a fluid is a squishy substance that is hard to grab hold of. If a solid body is in translation motion, the velocity of each part of the body is same but if a fluid is in motion, the velocity may be different at each location in the fluid. It's a question to how a moving fluid can be visualized so as to apply it in the fundamental physical principles. For a continuum fluid, one of the four models described below is to be constructed so as to apply it in the fundamental physical principles (Anderson, 1995).

1. Model of finite control volume fixed in space.
2. Model of finite control volume moving with fluid flow.

3. Model of an infinitesimally small fluid element fixed in space.

4. Model of an infinitesimally small fluid element moving with fluid flow.

The governing equations can be obtained in various different forms. For most application theory, the particular form of the equations makes little difference but however, for a given algorithm in CFD, the use of the equations in one form may lead to success, where as the use of an alternate form may result in different numerical results as incorrect results or instable results. Therefore, in the world of CFD, the various forms of the equations are of vital role in their application. Governing equations which comes from finite control volume are in integral form where as those originates from model of an infinitesimally small fluid element are in differential form. Fig.3.1 shows the generation of basics governing form used in CFD from fundamental physical principal.

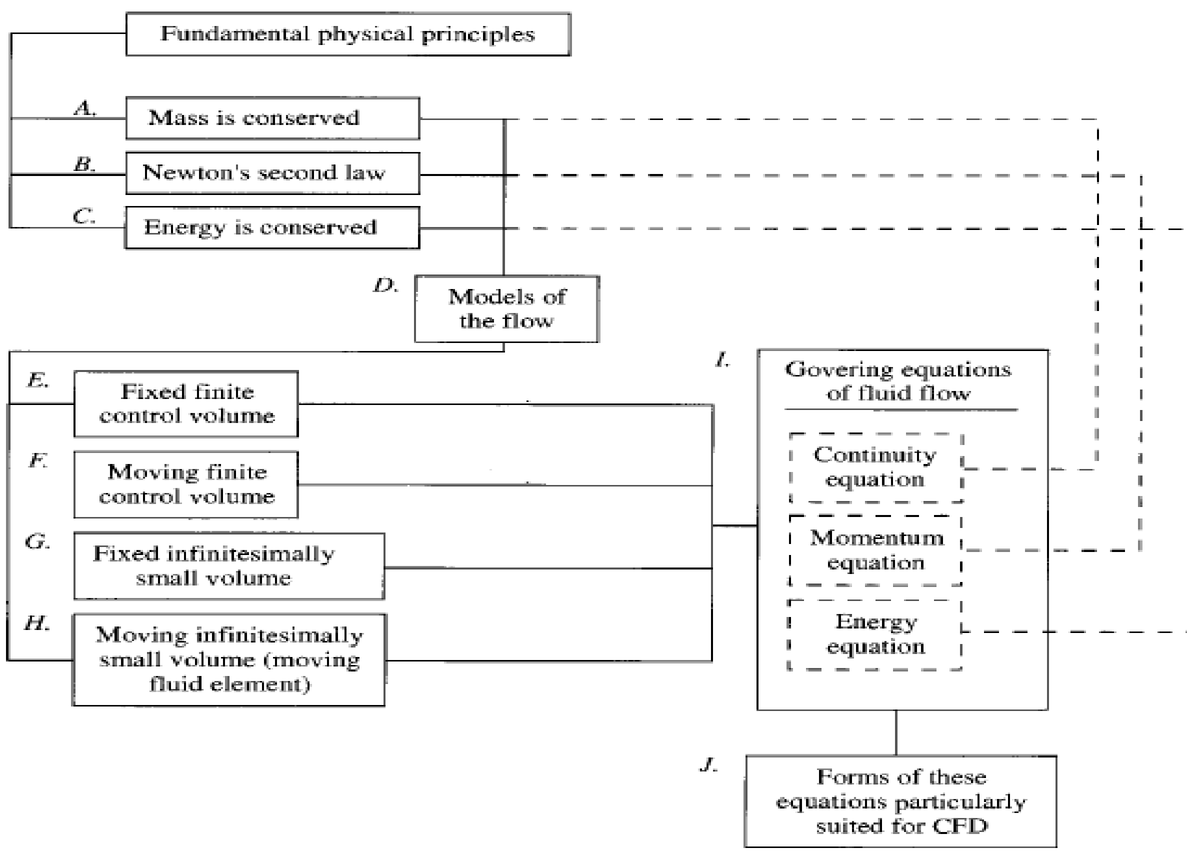

Fig. 3.1. Basics governing forms of CFD originated from physical principal (source- Anderson. J., 1995).

In the present work model of an infinitesimally small fluid element fixed in space were applied which is differential and conservation form. An Eulerian multi-fluid model has been adopted where gas, liquid and solid phases are all treated as continua, interpenetrating and interacting with each other everywhere in the computational domain. The pressure field is assumed to be shared by all the three phases, in proportion to their volume fraction. The motion of each phase is governed by respective mass and momentum conservation equations.

Continuity equation:

$$\frac{\partial(\varepsilon_k \rho_k)}{\partial t} + \nabla(\rho_k \varepsilon_k \vec{u}_k) = 0 \tag{3.1}$$

Where ρ_k is the density and ε_k is the volume fraction of phase k =gas, solid, liquid and the volume fraction of the three phases satisfy the following condition.

$$\varepsilon_l + \varepsilon_g + \varepsilon_s = 1 \tag{3.2}$$

Momentum equations: f*or liquid phase*:

$$\frac{\partial(\rho_l \varepsilon_l \vec{u}_l)}{dt} + \nabla(\rho_l \varepsilon_l \vec{u}_l \vec{u}_l) = -\varepsilon_l \nabla P + \nabla(\varepsilon_l \mu_{eff,l}(\nabla \vec{u}_l + (\nabla \vec{u}_l)^T)) + \rho_l \varepsilon_l g + M_{i,l} \tag{3.3}$$

Momentum equations: f*or gas phase*:

$$\frac{\partial(\rho_g \varepsilon_g \vec{u}_g)}{dt} + \nabla(\rho_g \varepsilon_g \vec{u}_g \vec{u}_g) = -\varepsilon_g \nabla P + \nabla(\varepsilon_g \mu_{eff,g}(\nabla \vec{u}_g + (\nabla \vec{u}_g)^T)) + \rho_g \varepsilon_g g + M_{i,g} \tag{3.4}$$

Momentum equations: f*or solid phase*:

$$\frac{\partial(\rho_s \varepsilon_s \vec{u}_s)}{dt} + \nabla(\rho_s \varepsilon_{s s} \vec{u}_s \vec{u}_s) = -\varepsilon_s \nabla P + \nabla(\varepsilon_s \mu_{eff,s}(\nabla \vec{u}_s + (\nabla \vec{u}_s)^T)) + \rho_s \varepsilon_s g + M_{i,s} \tag{3.5}$$

Where P is the pressure and μ_{eff} is the effective viscosity. The second term on the R.H.S of solid phase momentum Eq. (3.5) is the term that accounts for additional solid pressure due to solid collisions. The terms $M_{i,l}$, $M_{i,g}$, and $M_{i,s}$ of the above momentum equations represent the interphase force term for liquid, gas and solid phase, respectively. All these equations have been iteratively solved by FLUENT, which is a finite volume solver that uses discrete volumes to solve complex fluid flow problems.

3.8.1. Closure law for turbulence

The effective viscosity of the liquid phase is calculated by the equation given as

$$\mu_{eff,l} = \mu_l + \mu_{Tl} + \mu_{tg} + \mu_{ts} \tag{3.6}$$

Where μ_l is the liquid viscosity and $\mu_{T,l}$ is the liquid phase turbulence viscosity or shear induced eddy viscosity, which is calculated based on the *k*–*ε* model of turbulence written as

$$\mu_{Tl} = C_\mu \rho_l \frac{k^2}{\varepsilon} \tag{3.7}$$

Where the values of *k* and *ε* are obtained directly from the differential transport equations for the turbulence kinetic energy and turbulence dissipation rate μ_{tg} and μ_{ts} represent the gas and solid phase induced turbulence viscosity, respectively, and are given by the equations proposed by Sato et al. (1981) as

$$\mu_{tg} = c_{\mu p} \rho_l \varepsilon_g d_b \,|\vec{u}_g - \vec{u}_l|\tag{3.8}$$

$$\mu_{ts} = c_{\mu p} \rho_l \varepsilon_s d_p \,|\vec{u}_s - \vec{u}_l| \tag{3.9}$$

3.8.2. Interphase drag force

For fluid-fluid flows, each secondary phase is assumed to form droplets or bubbles. This has an impact on how each of the fluids is assigned to a particular phase. For example, in flows where there are unequal amounts of two fluids, the predominant fluid should be modeled as the primary fluid, since the sparser fluid is more likely to form droplets or bubbles. The exchange coefficient for these types of bubbly, liquid-liquid or gas-liquid mixtures can be written in the following general form as

$$K_{pq} = \frac{\alpha_q \alpha_p \rho_p f}{\tau_p} \tag{3.10}$$

Where f is the drag function, is defined differently for the different exchange-coefficient models and τ_p, is the particulate relaxation time defined as

$$\tau_p = \frac{\rho_p d_p^2}{18\mu_q} \tag{3.11}$$

Where d_p is the diameter of the bubbles or droplets of phase p. Nearly all definitions of f include a drag coefficient (C_D) that is based on the relative Reynold number (R_e). It is this drag function that differs among the exchange coefficient models. For the model of air–liquid interaction Schiller and Naumann drag model has been used which is described below.

$$f = \frac{C_D R_e}{24} \tag{3.12}$$

$$\begin{aligned} C_D &= 24(1+0.15R_e^{0.687})/R_e \qquad && R_e \le 1000 \\ &= 0.44 && R_e > 1000 \end{aligned} \tag{3.13}$$

The relative Reynolds number for the primary phase q and secondary phase p is obtained as

$$R_e = \frac{\rho_q d_p \left| \vec{\upsilon}_p - \vec{\upsilon}_q \right|}{\mu_q} \tag{3.14}$$

The relative Reynolds number for secondary phases p and r is obtained as

$$R_e = \frac{\rho_{rp} d_{rp} \left| \vec{\upsilon}_r - \vec{\upsilon}_p \right|}{\mu_{rp}} \tag{3.15}$$

Where $\mu_{rp} = \alpha_p \mu_p + \alpha_r \mu_r$ is the mixture viscosity of the phases p and r.

The inter-phase exchange coefficient between fluid and solid phases is obtained by Gidaspow drag model .It is combination of Wen and Yu model and the Ergun equation. In present work both solid – liquid and solid – air interphase drag modeling done by Gidaspow model, which is described below.

For $\alpha_l \leq 0.8$

$$K_{sl} = 150\frac{\alpha_s(1-\alpha_l)\mu_l}{\alpha_l d_s^2} + 1.75\frac{\rho_l \alpha_s \left|\overrightarrow{\upsilon_s} - \overrightarrow{\upsilon_l}\right|}{d_s} \tag{3.16}$$

3.8.3. Closure law for solid pressure

The solid phase pressure gradient results from normal stresses resulting from particle–particle interactions, which become very important when the solid phase fraction approaches the maximum packing. The model for solid pressure is constant viscosity model (CVM), where the solid phase pressure is defined only as a function of the local solid porosity using empirical correlations and the dynamic shear viscosity of the solid phase is assumed constant. The constitutive equation for CVM model given by Gidaspow (1994) is as

$$\nabla P_s = G(\varepsilon_s)\nabla\varepsilon_s \tag{3.17}$$

where $G(\varepsilon_s)$ is the elasticity modulus and it is proposed by Bouillard et al. (1989) as

$$G(\varepsilon_s) = G_0 \exp(c(\varepsilon_s - \varepsilon_{sm})) \tag{3.18}$$

where G_0 is the reference elasticity modulus, c is the compaction modulus and ε_{sm} is the maximum packing parameter.

3.8.4. Turbulence modeling

It is an unfortunate fact that no single turbulence model is universally accepted as being superior for all classes of problems. The choice of turbulence model will depend on considerations such as the physics encompassed in the flow, the established practice for a specific class of problem, the level of accuracy required, the available computational resources, and the amount of time available for the simulation. In present simulation the Standard κ-ε Model has been taken for turbulence modeling.

The standard κ-ε model is a semi-empirical model based on model transport equations for the turbulence kinetic energy (κ) and its dissipation rate (ε). The model transport equation for turbulence kinetic energy is derived from the exact equation, while the model transport equation for dissipation rate has been obtained using physical reasoning and bears little resemblance to its mathematically exact counterpart.

The turbulence kinetic energy and its rate of dissipation are obtained from the following transport equations.

$$\frac{\partial}{\partial t}(\rho\kappa)+\frac{\partial}{\partial\chi_i}(\rho\kappa\upsilon_i)=\frac{\partial}{\partial\chi_j}[(\mu+\frac{\mu_t}{\sigma_k})\frac{\partial\kappa}{\partial\chi_i}]+G_k+G_b-\rho\varepsilon-Y_M+S_\kappa \qquad (3.19)$$

And

$$\frac{\partial}{\partial t}(\rho\varepsilon)+\frac{\partial}{\partial\chi_i}(\rho\varepsilon\upsilon_i)=\frac{\partial}{\partial\chi_j}[(\mu+\frac{\mu_t}{\sigma_\varepsilon})\frac{\partial\varepsilon}{\partial\chi_j}]+C_{1\varepsilon}\frac{\varepsilon}{\kappa}(G_k+C_{3\varepsilon}G_b)-C_{2\varepsilon}\rho\frac{\varepsilon^2}{k}+S_\varepsilon \qquad (3.20)$$

In these equations, G_κ represents the generation of turbulence kinetic energy due to the mean velocity gradients, G_b is the generation of turbulence kinetic energy due to buoyancy, Y_M represents the contribution of the fluctuating dilatation in compressible turbulence to the overall dissipation rate, $C_{1\varepsilon}$, $C_{2\varepsilon}$ and $C_{3\varepsilon}$ are constants. σ_κ and σ_ε are the turbulent Prandtl numbers for turbulence kinetic energy and dissipation rate respectively. S_κ and S_ε are user-defined source terms where C_μ is a constant.

The turbulent viscosity, (μ_t) is computed by combining κ and ε as follows

$$\mu_t=\rho C_\mu\frac{\kappa^2}{\varepsilon} \qquad (3.21)$$

Where C_μ is a constant

3.9. Discritization

To obtain an approximate solution numerically, we have to use a discritization method which approximates the differential equations by a system of algebraic equations, which can then be further solved. The approximations are applied to small domains in space and time so the numerical solutions provide results at discrete locations in space and time. It concerns the process of transferring continues models and equations into discrete counterparts. This process is usually carried out as a first step toward making them suitable for numerical evaluation and implementation on digital computers. For a given differential equation, there can be several different ways to derive the discretized equations such as finite difference, finite volume and finite element to achieve the stable solution as explained by Fig. 3.2. Finite volume methods ensure integral conservation of mass and momentum over any group of control volumes. The accuracy of numerical solutions is dependent on the quality of discritization used. Each type of method yields the same solution if the grid is very fine, however, some methods are more suitable to some class of problems than others (Ferziger., 2002). In present work discritization based on finite volume method has been used.

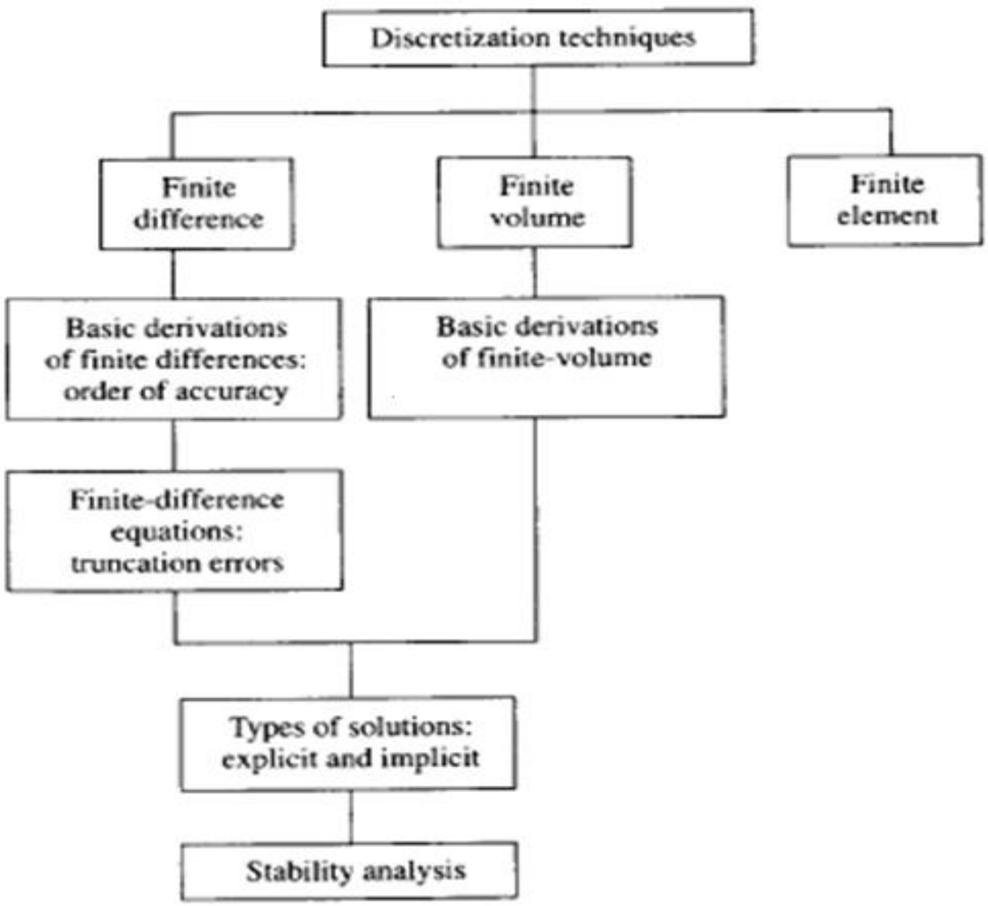

Fig. 3.2. Elements of discritization technique (Source: Anderson., 1995).

Fluent uses Finite volume method (FVM) of discritization to convert the governing equations to algebraic equations that can be solved numerically. This is the "classical" or standard approach used most often in commercial software and research codes. The governing equations are solved on discrete control volumes. FVM recasts the PDE's (Partial Differential Equations) of the Naviour-Stokes equation in the conservative form and then discretize this equation. The solution domain is subdivided into a finite number of contiguous control volumes (CV), where conservation equations are applied. At the centroid of each CV, there lies a computational node at which the variable values are to be calculated. Interpolation is used to express variable values at the CV surface in terms of nodal (CV center) values. Surface and volume integrals are approximated using suitable quadrature formulae. The integration approach yields a method that is inherently conservative (i.e. quantities such as density remain physically meaningful). This is demonstrated by the following equation written in integral form for an arbitrary control volume *V* as

$$\frac{\partial}{\partial t}\iiint Q\,dV + \iint F\,d\mathbf{A} = 0 \tag{3.22}$$

Where *Q* is the vector of conserved variables, *F* is the vector of fluxes, *V* is the cell volume, and *A* is the cell surface area. The FVM approach is the simplest to understand and to program and can accommodate any type of grid, so it is suitable for complex geometries. The grid defines only the control volume boundaries and need not be related to a coordinate system. There are three levels in solving the numerical equations by FV approach; these are the approximation, interpolation and differentiation. So it is the disadvantage that the higher than second order are more difficult to develop in 3-D by FV approach.

3.10. Computation of energy flows

In gas–liquid–solid fluidized beds, the input energy from the gas and liquid is distributed to the mean flow of the liquid, gas, and the solid phases. Also, a part of the input energy is used for liquid phase turbulence and some part of the energy gets dissipated due to the friction between the liquid and solid phases and the gas and liquid phases. Apart from these energy dissipation factors, some of the other energy losses due to solid fluctuations, collisions between particles, between particles and column wall are also involved in three-phase reactors. Since the present CFD simulation is based on Eulerian–Eulerian approach, these modes of energy dissipation could not be quantified. Hence, these terms are neglected in the energy calculation. In general, the difference between the input and output energy should account for the energy dissipated in the system (Panneerselvam et al., 2009). Thus, the energy difference in this work is calculated as

Energy difference = $E_I - E_{out} - E_T - Ee - E_{Bls} - E_{Blg}$ (3.23)

Where, E_I - energy entering in the fluidized bed

E_{out} - energy leaving the fluidized bed by liquid and gas phase.

E_T - energy gained by solid phase.

E_e - energy dissipated by liquid phase turbulence.

E_{Bls}- energy dissipated due to friction at liquid solid interface.

E_{Blg} - energy dissipated due to friction at gas liquid interface.

Energy entering the fluidized bed (*E*$_i$) by the incoming liquid and gas - The energy entering the fluidized bed due to the incoming liquid and gas flow is given as

$$E_i = \frac{\pi}{4} D^2 Hg(V_l + V_g)(\varepsilon_s \rho_s + \varepsilon_l \rho_l + \varepsilon_g \rho_g) \tag{3.24}$$

where *D* is the diameter of the column, *H* is the expanded bed height, V_l is superficial liquid velocity, V_g is the gas superficial velocity, ε_l,ε_g,ε_s are the liquid, gas and solid volume fraction, and ρ_l, ρ_g, ρ_s are the liquid, gas and solid densities, respectively.

Energy leaving the fluidized bed (*E*$_{out}$) by the out flowing liquid and gas - The liquid and the gas leaving the bed possess both potential energy and kinetic energy by virtue of its expanded bed height and are given as

$$E_{out} = E_{pl}+E_{pg}+E_{kl}+E_{kg} \tag{3.25}$$

$$E_{pl} = \frac{\pi}{4} D^2 HV_1 \rho_1 g \tag{3.26}$$

$$E_{Pg} = \frac{\pi}{4} D^2 HV_g \rho_g g \tag{3.27}$$

$$E_{kl} = \frac{1}{2} \rho_l \frac{\pi}{4} D^2 V_l^3 \tag{3.28}$$

$$E_{kg} = \frac{1}{2} \rho_g \frac{\pi}{4} D^2 V_g^3 \tag{3.29}$$

Energy gained by the solid phase (E_T) - The energy gained by the solids for its upward motion in the center region is the sum of the potential energy and kinetic energy of the solids and are written as

$$E_T = E_{PS} + E_{ks} \tag{3.30}$$

$$E_{PS} = \rho_s g H \frac{\pi}{4} D_C^2 v_s \tag{3.31}$$

$$E_{ks} = \frac{1}{2}\rho_s \frac{\pi}{4} D_c^2 v_s^3 \tag{3.32}$$

Where v_s is the averaged solid velocity in the center region, and D_c is the diameter of the center region.

Energy dissipation due to liquid phase turbulence (E_e) - Since k–ε model for turbulence is used in this work, the energy dissipation rate per unit mass is given by the radial and axial variation of ε. Hence, the energy dissipated due to liquid phase turbulence is calculated as

$$E_e = \int_0^R \int_0^H \int_0^{2\pi} \varepsilon dr\, dz\, d\theta \tag{3.33}$$

Energy dissipation at the liquid–solid interface (E_{Bls})

The net rate of energy dissipation due to friction at the liquid–solid interface is calculated based on the total drag force between the liquid and solid phase and is given by

$$E_{Els} = \frac{\pi}{4} D^2 \varepsilon_g g(\rho_c - \rho_g)(1-\varepsilon_g)^{4.78} V_s \tag{3.34}$$

Energy dissipation at the gas–liquid interface (E_{Bgl})

The net rate of energy dissipation due to friction at the gas-liquid interface is calculated based on the total drag force between the gas and the liquid phase and is given by

$$E_{Bgl} = \frac{\pi}{4} D^2 H \varepsilon_g g(\rho_c - \rho_g)(1-\varepsilon_g) V_{bs} \tag{3.35}$$

Chapter 4
Numerical Methodology

No knowledge can be certain, if it is not based
Upon mathematics or some other knowledge which
is itself based upon the mathematical sciences

Leonardo da vinci (1425-1519)

Chapter–4

Numerical Methodology

In the present work of three phase fluidization solid material is the glass beads of uniform size which are initially in static condition inside the fluidized bed column and forms a desired height in the bed .The water i.e. liquid phase and air are introduced from the bottom of the column so that the fluidization starts. The model equations described in Chapter- 3 are solved using the commercial CFD software package FLUENT 6.2.16. Fig. 4.1 shows the general procedure for the simulation using FLUENT software.

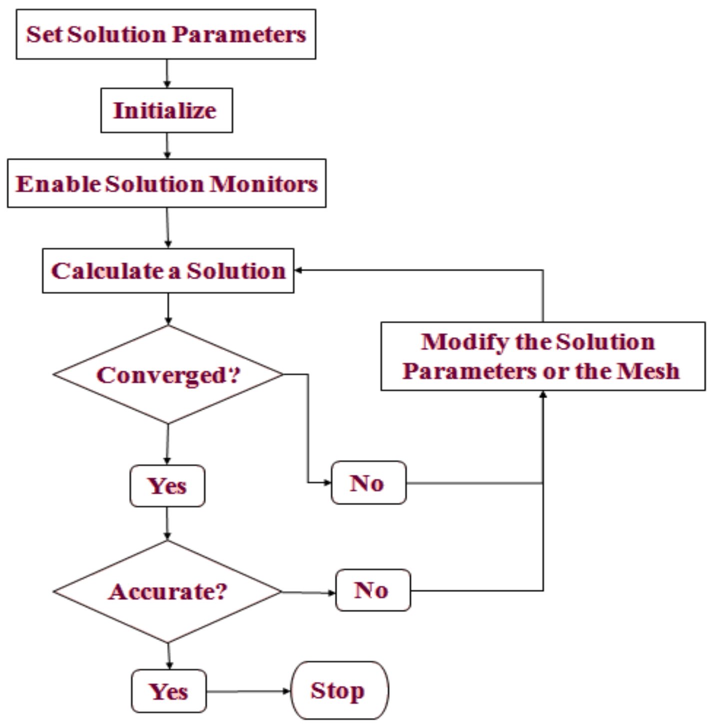

Fig. 4.1. Flowchart showing the general procedure for the simulation using FLUENT.

4.1. Geometry and mesh

The first step in CFD simulation of fluidized bed column is preprocessor, which has been done by GAMBIT tools, to design the problem in geometrical configuration and mesh the geometry. Before fluid flow problems can be solved, FLUENT needs the domain in which the flow takes place to evaluate the solution. The flow domains as well as the grid generation into the specific domain have been created in GAMBIT which is shown in Fig. 4.2. GAMBIT has been used to create the geometry of the cylindrical with desired dimensions. Both the two dimensional and three dimensional geometry have been created and meshed to form the grid. In 3D geometry hexahedral meshing has been done with element type hex / wedge. In 1.88 m height column dividing with 33 interval counts using cooper scheme 14760 cells, 47062 faces, and 17738 nodes have been created. In 1.5 m height column with dividing in 25 interval counts using cooper scheme 7936 cells, 25484 faces and 9750 nodes and for 2.5 m height column with dividing in 51 interval counts 11770 cells, 37239 faces and 13824 nodes have been created. In 2D geometry of 1.88 m height column dividing with 360 vertical count and 40 horizontal count 14400 cells, 29200 faces and 14801 nodes have been created. After meshing, the FLUENT 5/6 solver needs to be specified so that GAMBIT knows what types of boundary conditions are allowed. The boundary conditions such as velocity-inlet, pressure outlet, wall and default interior have been set. Then the grid has been exported as a mesh file from GAMBIT to be used in FLUENT for solution.

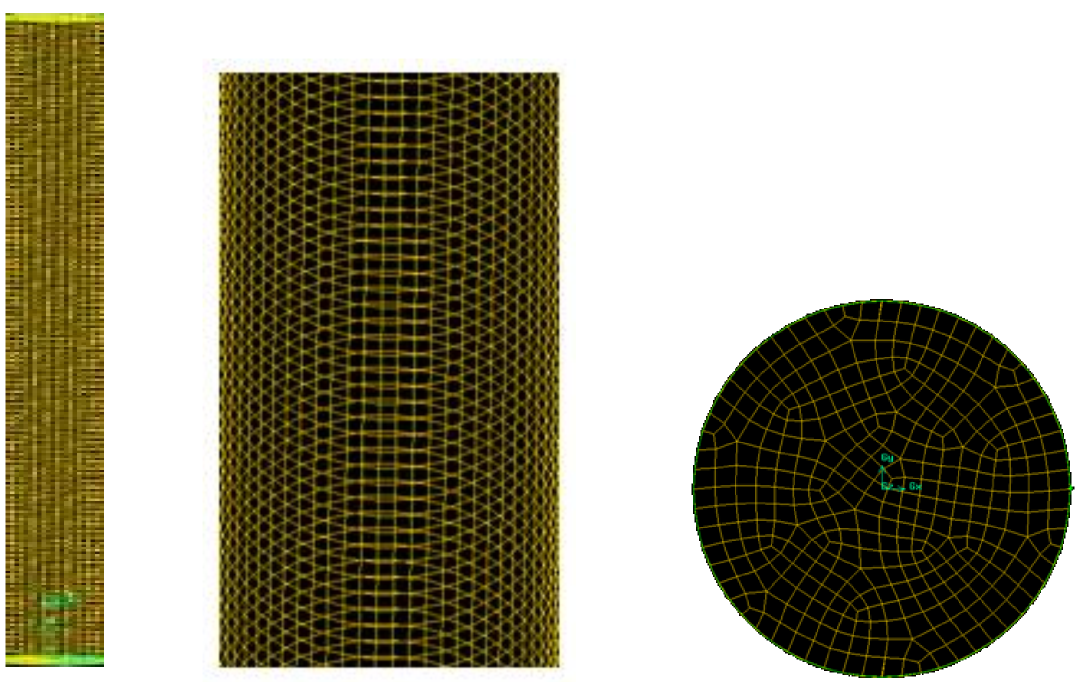

(A) (B) (C)

Fig. 4.2. Hexahedral meshing of cylindrical column (A) Front view (B) Zoom View of meshing (C) Top view.

4.2. Boundary and initial conditions

In order to obtain a well-posed system of equations, reasonable boundary conditions for the computational domain have to be implemented. Inlet boundary condition is a uniform liquid and gas velocity at the inlet and outlet boundary condition is the pressure boundary condition, which is set as1.013×105 Pa. Wall boundary conditions are no-slip boundary conditions for the liquid phase and free slip boundary conditions for the solid phase and the gas phase. The restitution coefficient for solid – solid has been taken default value of 0.9. The higher viscous effect and higher velocity gradient near the wall have been dealt with the standard wall function method. For patching a solid volume fraction, the solid in the part of the column up to which the glass beads were initially fed has been used. At initial condition the solid volume fraction of 0.59 of the static bed height of column has been used and the volume fraction of the gas at the inlet is based on the inventory. Table 4.1 shows the boundary and initial conditions for different fluidized bed column.

Table 4.1: Physical and process parameters in different column for simulation.

Physical and process parameters	**Cylindrical column (I)**	**Cylindrical Column (II)**	**Cylindrical column(III)**
Diameter of column (m)	0.1	0.1	0.254
Height of column (m)	1.88	1.5	2.5
Density of solid (kg/m^3)	2470	2475	2470
Mean particle size (mm)	2.18, 4.05	3	2.3, 4.05
Initial bed height (m)	0.213, 0.367, 0.267	0.35	0.267, 0.39
Initial solid holdup	0.59	0.59	0.59
Inlet air velocity (m/s),	0.02 -0.12	0.069, 0.11	0.02123, 0.04
Inlet liquid velocity (m/s)	0.03 -0.14	0.065	0.06, 0.09

The main focus for analysis is based on cylindrical column (I) and parameters which are varied in 1.88 m height fluidized bed for present simulation and hydrodynamic study are presented in Table 4.2.

Table 4.2: Parameters Varied in the simulation of 1.88 m height fluidized bed.

S.No	Water Inlet velocity (m/sec)	Air inlet velocity (m/sec)	Glass bead mean dia (mm)	Initial solid bed height (m)
1	0.10616	0.0637	2.18	0.213
2	0.10616	0.0800	2.18	0.213
3	0.10616	0.1100	2.18	0.213
4	0.10616	0.02548	2.18	0.213
5	0.10616	0.05096	2.18	0.213
6	0.0637	0.02548	2.18	0.213
7	0.0637	0.05096	2.18	0.213
8	0.0637	0.01274	2.18	0.213
9	0.03185	0.02548	2.18	0.213
10	0.05	0.02548	2.18	0.213
11	0.0637	0.02548	2.18	0.213
12	0.09	0.02548	2.18	0.213
13	0.105	0.02548	2.18	0.213
14	0.04	0.02123	4.05	0.267
15	0.06	0.02123	4.05	0.267
16	0.09	0.02123	4.05	0.267
17	0.11	0.02123	4.05	0.267
18	0.13	0.02123	4.05	0.267
19	0.04	0.02123	2.18	0.213
20	0.06	0.02123	2.18	0.213
21	0.09	0.02123	2.18	0.213
22	0.11	0.02123	2.18	0.213
23	0.13	0.02123	2.18	0.213
24	0.0637	0.11	2.18	0.213

4.3. Solution techniques

In FLUENT, solver is set as segregated which solves the equations individually. Unsteady state has been formulated as 1st order implicit condition and cell based gradient option has been taken.

The discretization scheme for momentum, volume fraction, turbulence kinetic energy and turbulence dissipation rate all has been taken as first order upwind.

The solution procedure involves the following steps:

1. Generation of suitable grid system.
2. Conversion of governing equation into algebraic equations.
3. Selection of discretization schemes.
4. Formulation of the discretized equation at every grid location.
5. Formulation of pressure equation.
6. Development of a suitable iteration scheme for obtaining a final solution.

The under relaxation factors have been taken for solution control in different flow quantities as pressure = 0.3, density = 1, body forces = 1, momentum = 0.2 - 0.4, volume fraction = 0.5, granular temperature = 0.2, turbulent kinetic energy = 0.8, turbulent dissipation rate = 0.8 and turbulent viscosity =1. For pressure-velocity coupling Phase Coupled SIMPLE method has been chosen. The solution has been initialized from all zones. The convergence criteria are preset conditions for the residuals that determine when an iterative solution is converged. For any set of convergence criteria, the assumption is that the solution is no longer changing with more iteration and when the condition is reached there is an overall mass balance throughout the domain. In present work the convergence criteria of all the residual has been taken as 0.001 and iterations have been carried out with time step size of 0.001. The residual plot of progress of the simulation is shown in Fig. 4.3.

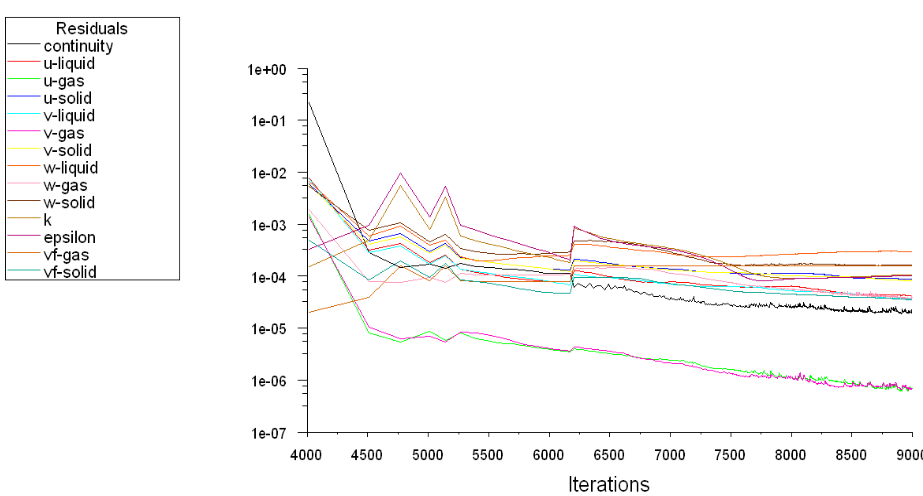

Fig. 4.3. Plot of residual proceeding with iteration for simulation in FLUENT.

Chapter 5

Results And Discussion

Results and discussion

The simulated results of different fluidized bed system investigated have been presented in this chapter. Contours of volume fraction of solid with respect to time in Simulation has been shown in Fig. 5.1 with the inlet air velocity 0.02548 m/s and the inlet water velocity of 0.0637 m/s for 1.88 m height column. For this case the initial solid bed height of 21.3 cm and glass beads of size 2.18 mm has been used.

.

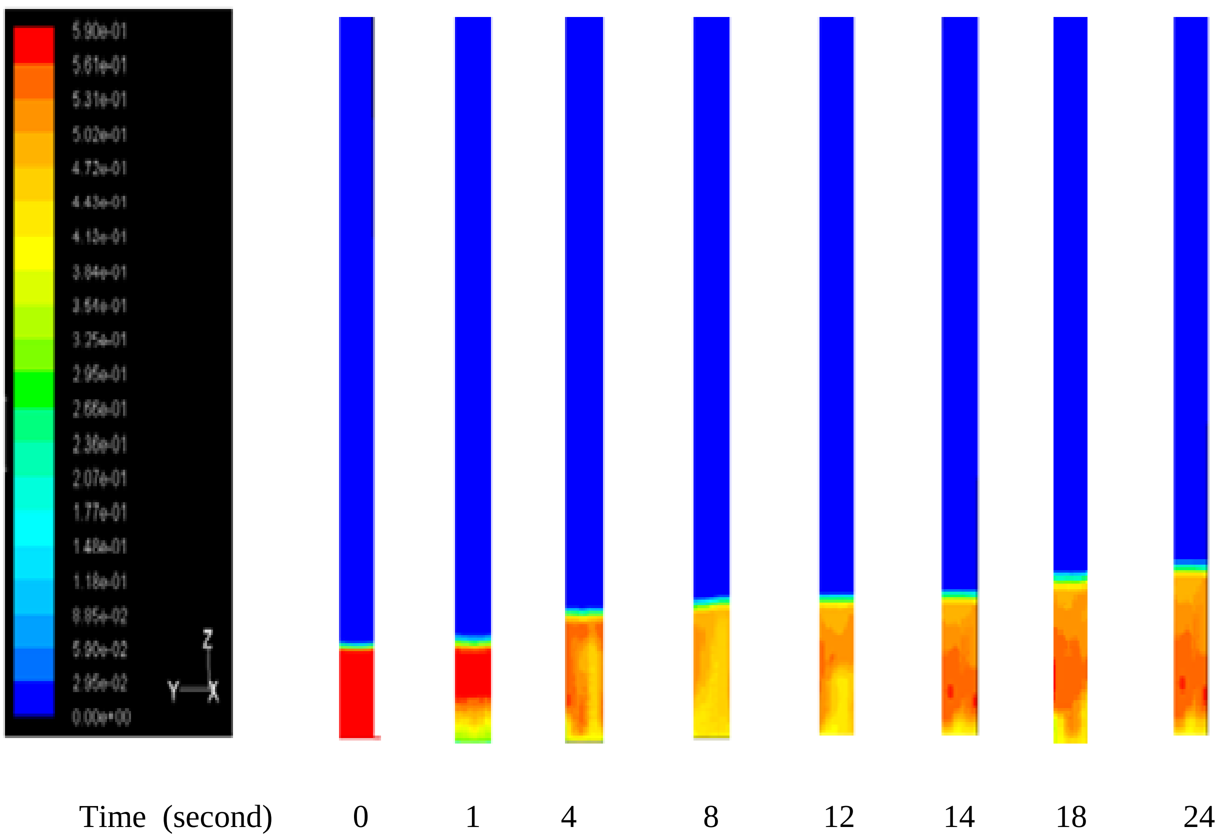

Fig. 5.1. Contours of volume fraction of solid in 1.88 m height fluidized bed at [V_l = 0.0637m/s, V_g = 0.02548 m/s, H_s = 0.213 m, D_p = 2.18 mm].

Initially no flow in bed is observed, while simulating the fluidized bed the profile of bed changes with time. But after some time no significant change in the profile is observed. This indicates that the fluidized bed has come to a quasi steady state and we take all the information for results from this. The simulations have been carried out till the system reached the quasi-steady state i.e., the averaged flow variables are time independent; this can be achieved by monitoring the expanded bed height or phase volume fractions. It can be observed from the figure (Fig. 5.1) that, the bed profile is almost the same between 18 – 24 second of simulation time while simulations continued for 25 – 30 second and the averages over the last 10 s were used in the analysis.

5.1. Phase dynamics

Solid, liquid and gas phase dynamics have been represented in the form of contours plots Contours of volume fractions of solid, liquid and gas in the column obtained at water velocity of 0.06 m/s; air velocity of 0.04 m/s; initial static bed height of 0.39 m and glass beads of diameter 2.3 mm in 2.5 m height column after the achieving quasi steady state have been shown in Fig. 5.2.

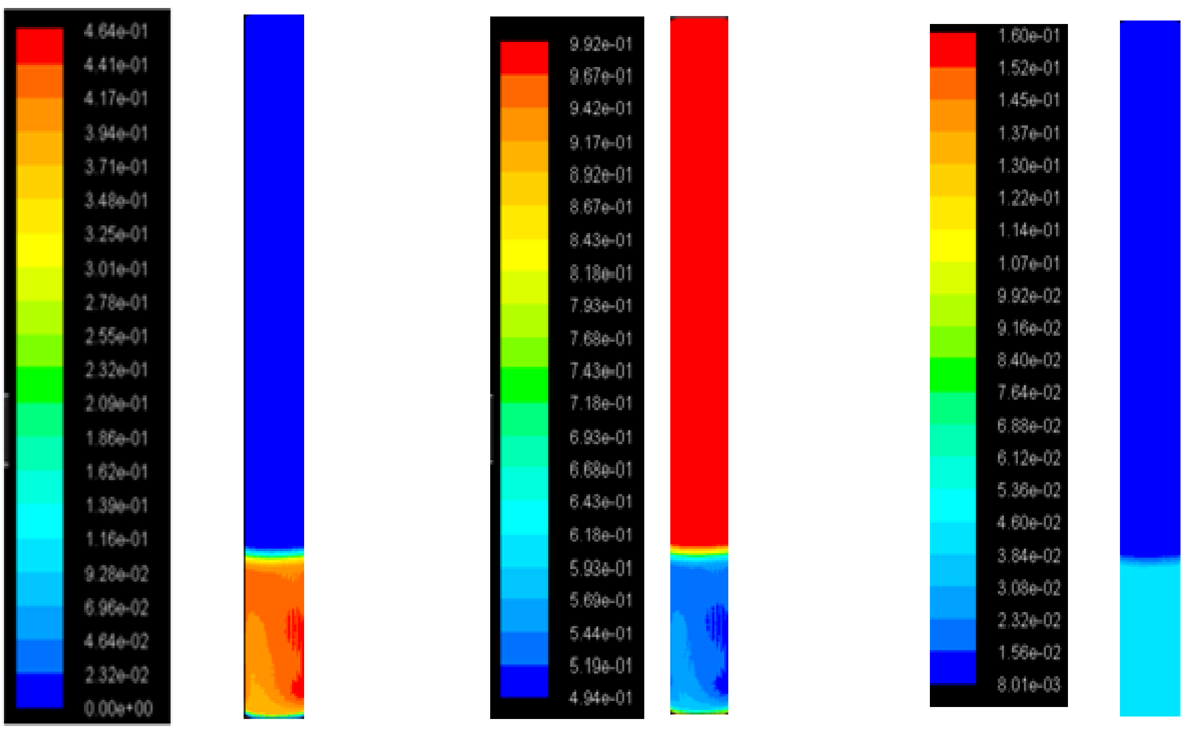

Solid Liquid Gas

Fig. 5.2. Contours of volume fraction of solid, liquid and gas in 2.5 m height fluidized bed at [V_l = 0.06 m/s, V_g = 0.04 m/s, H_s = 0.39 m, D_p = 2.3 mm].

The colour scale given to the left of each contours gives the value of volume fraction corresponding to the colour The contours for glass beads illustrates that bed is in fluidized condition. The contours for water illustrates that volume fraction of water (liquid holdup) is less in fluidized part of the column compared to remaining part. The contour for air illustrates that gas holdup is significantly more in fluidized part of the bed compared to remaining part.

5.2. Velocity Profiles of gas, liquid and solid

In three phase fluidization velocity of solid, liquid and gas changes with time and location in the bed. The velocity vector of glass beads of size 2.18 mm with the air inlet velocity of 0.11 m and the water inlet velocity of 0.0637 m at the solid static bed height of 0.213 m has been shown in Fig. 5.3. Solids flow structure in three phase-fluidized beds shows a single circulation pattern, where there is a central fast bubble flow region in which the solids move upward and a relatively bubble free wall region where the solids flow downwards. It can be clearly observed that the velocity of solid at the bottom is small and at top all the velocity vectors are showing downward trend. Because no glass beads are present in the upper section, so no velocity vectors can be seen at top.

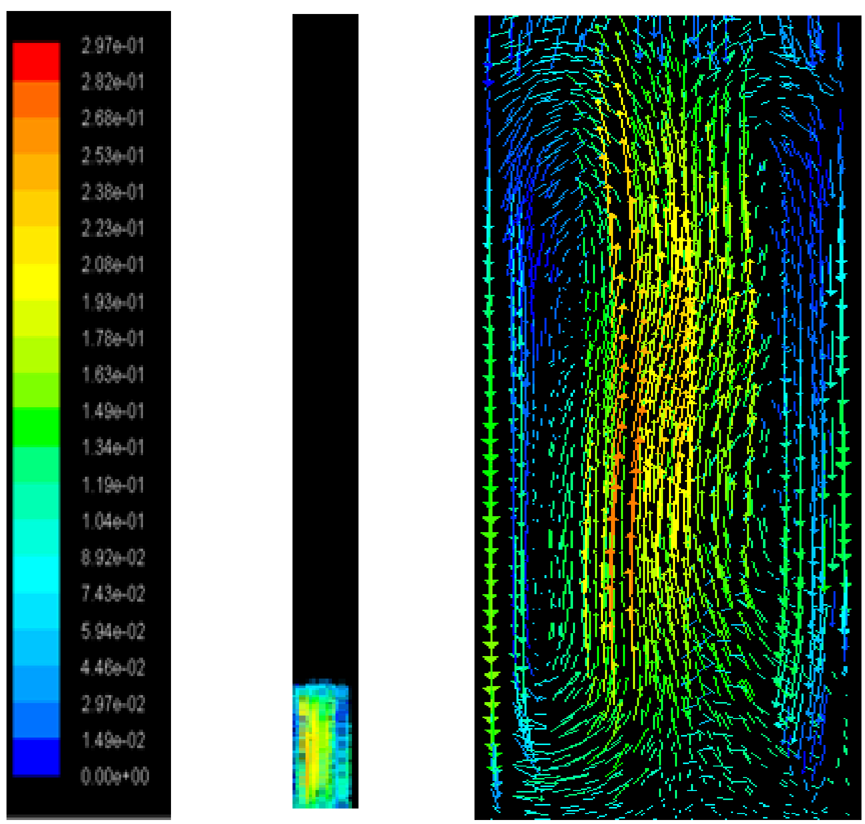

Actual *(Magnified view)*

Fig. 5.3. Velocity vector of glass beads in 1.88 m height fluidized bed (actual and magnified) at [V_l = 0.0637 m/s, V_g = 0.11 m/s, H_s = 0.213 m, D_p = 2.18 mm].

The velocity profiles of solid, liquid and gas with glass beads of size 2.18 mm, inlet water velocity of 0.10616 m/s and inlet air velocity of 0.08 m/s have been shown in Fig. 5.4, Fig. 5.5 and Fig. 5.6 respectively. The lines at different bed height along radial direction created in 3D model for calculating the velocity profile. All these lines represent the velocity magnitude at respective bed height along radial direction.

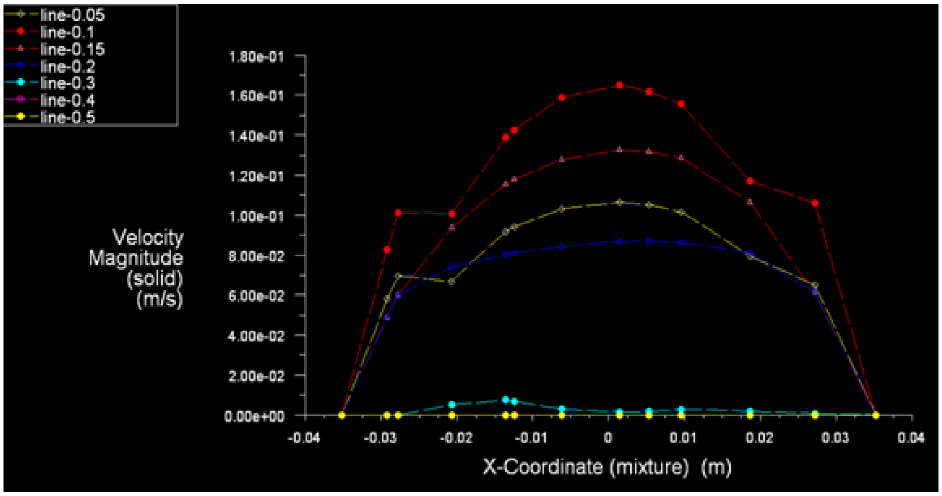

.

Fig. 5.4. Velocity profiles of glass beads with different bed height along radial direction in 1.88 m height fluidized bed at [V_l = 0.10616 m/s, V_g = 0.08 m/s, H_s = 0.213 m, D_p = 2.18 mm].

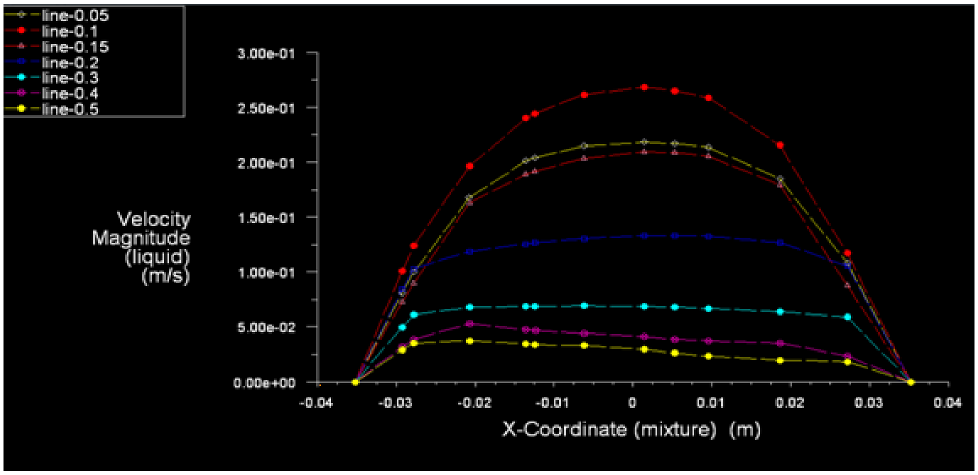

Fig. 5.5. Velocity profiles of water with different bed height along radial direction in 1.88 m height fluidized bed at [V_l = 0.10616 m/s, V_g = 0.08 m/s, H_s = 0.213 m, D_p = 2.18 mm].

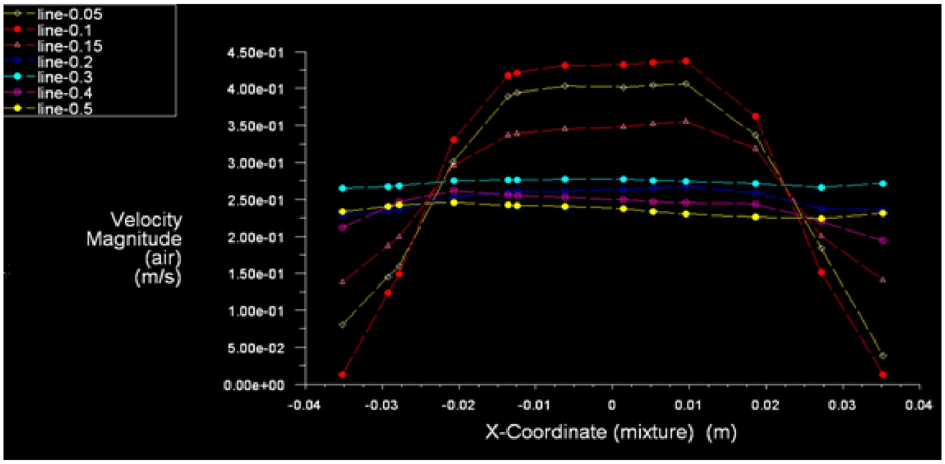

Fig. 5.6. Velocity profiles of air with different bed height along radial direction in 1.88 m height fluidized bed at [V_l = 0.10616 m/s, V_g = 0.08 m/s, H_s = 0.213 m, D_p = 2.18 mm].

The velocity profile of glass beads shows the changes in velocity magnitude along radial direction of cylindrical column at different bed heights. At the bed height of 0.05 m, glass beads velocity profile shows the maximum velocity along radial direction is 0.1 m/sec. The velocity of glass beads then increased and attained the maximum velocity of 0.16 m/sec at bed height of 0.1 m. On small further increase in bed height the velocity of glass beads decreases and finally velocity becomes close to zero at 0.3 m and above this the velocity magnitude is zero since no solid particles are there. The velocity Profile also shows that the magnitude of velocity is more in center region and at wall the velocity is zero. The velocity profile of water shows the parabolic pattern for a fully developed flow this kind of parabolic pattern is must for laminar flow. The maximum liquid velocity found in the profile to be 0.26 m/sec at bed height of 0.1 m. Then the liquid velocity decreases with the bed height above 0.1 m and there is almost same velocity (0.03 – 0.05 m/s) along radial direction has been found when the bed height is between (0.3 -0.5 m).

The maximum gas velocity found in the profile to be 0.42m/sec at bed height of 0.1 m. Then the gas velocity decreases with the bed height after 0.1 m and there is almost same velocity (0.23 – 0.26 m/s) along radial direction has been found when the bed height is between (0.3 -0.5 m).

5.2.1. Change in velocity profile with simulation time

Velocity magnitudes of water and solid glass beads with time has been obtained at the inlet water velocity of 0.08 m/s and the inlet air velocity of 0.09 m/sec by taking mean area weighted at bed height of 0.35 m are shown in Fig.5.7 and Fig.5.8 respectively. The initial inlet velocity of liquid in the column at time of zero second is 0.08 m/s and found to be 0.11 m/sec at the time of 6^{th} second. The maximum velocity of liquid has been found to 0.124 m/sec at time of 7.2 second as shown in Fig. 5.7.

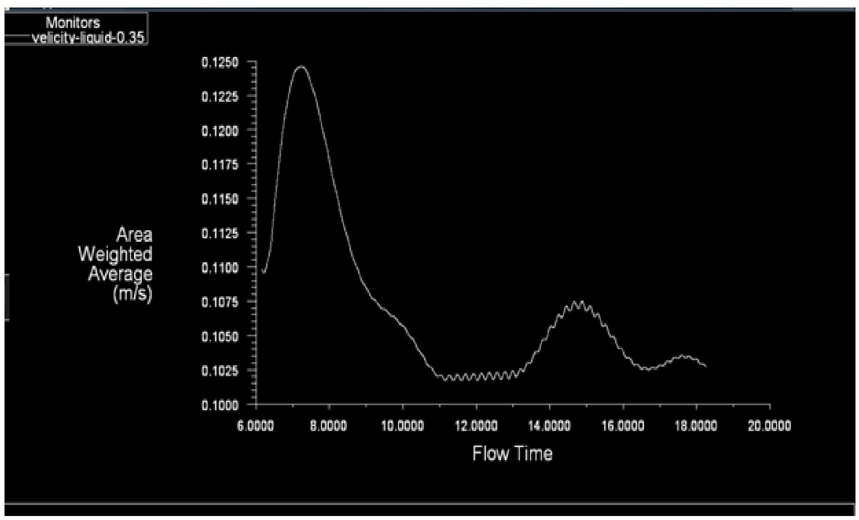

Fig.5.7. Plot of velocity magnitude of water at bed height of 0.35 m versus flow time in 1.88 m height fluidized bed at [V_l = 0.08 m/s, V_g = 0.09 m/s, H_s = 0.213 m, D_p = 2.18 mm].

The velocity of glass beads initially at the static condition in the column at time of zero second and is found to be 0.0650 m/sec at the time of 6^{th} second. Maximum velocity of glass beads has been found as 0.0930 m/sec at time of 7.2 second as shown in Fig. 5.8. Both liquid and solid velocities in the fluidized bed have been found to increase with time at the beginning of simulation and then it decreases showing an oscillatory behavior with decreasing amplitude. It means that for a given initial condition the velocity will reach the maximum only once after starting the fluidization.

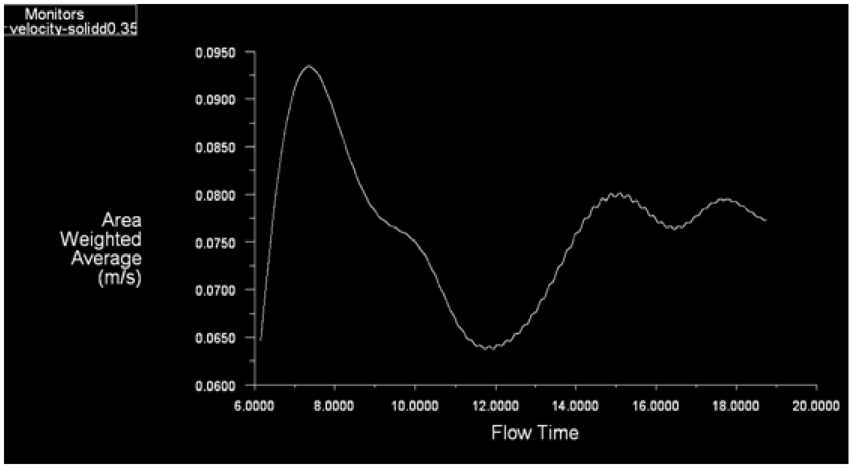

Fig.5.8. Plot of velocity magnitude of solid glass beads at height of 0.35 m versus flow time in 1.88 m height fluidized bed at [V_l = 0.08 m/s, V_g = 0.09 m/s, H_s = 0.213 m, D_p = 2.18 mm].

5.2.2. Comparison of gas, liquid and solid velocities

In three phase fluidization the velocity of all phases depends on each other interactions, which is complex in nature. The comparison of the velocity of all phases with the height of cylindrical column has been plotted in Fig. 5.9.

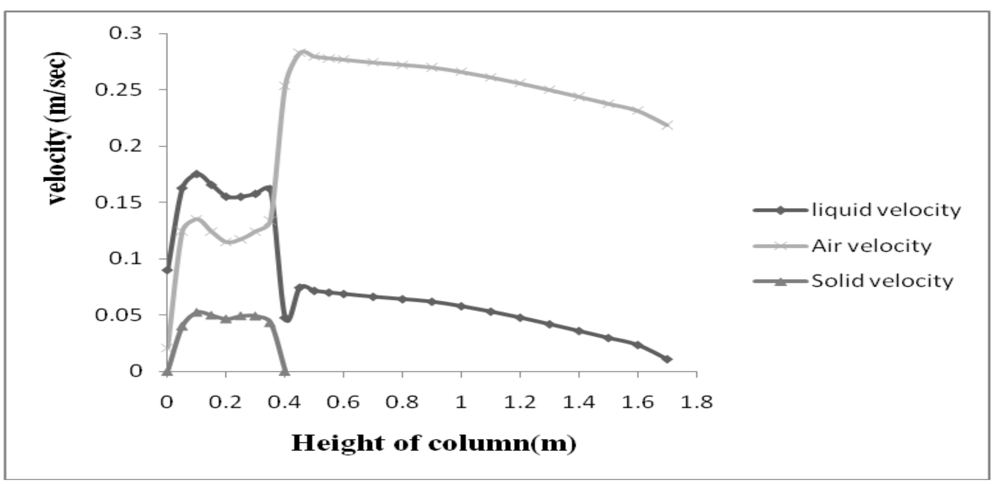

Fig. 5.9. Comparison of gas, solid and liquid velocities in 1.88 m height fluidized bed at [V_l = 0.09 m/s, V_g = 0.02123 m/s, H_s = 0.267 m, D_p = 4.05 mm].

The initial solid static bed height of 0.267 m; particle size of 4.05mm; air velocity of 0.02123 m/sec and water velocity of 0.09 m/sec have taken for comparison. The velocities of all the phases are fluctuating in the fluidized region. There is the sharp increase in air velocity and sharp decrease in liquid velocity just above the fluidized region of column. The velocities of both air and liquid have been found to decrease constantly on further increase in height of column. The maximum air velocity in column has been found as 0.27m/sec.

5.2.3. Axial solid velocity of experimental work

The experimental work of (Kiared et al., 1999) has been predicted with simulation and results for axial solid velocity profile with radial position shown in Fig. 5.10. For this simulation, the liquid superficial velocity 0.065m/s; gas superficial velocity 0.069m/s; glass beads of size 3mm; initial static bed height of 0.35 m and height of cylindrical column 1.5 m has been taken. The simulation result is in agreement with experimental work.

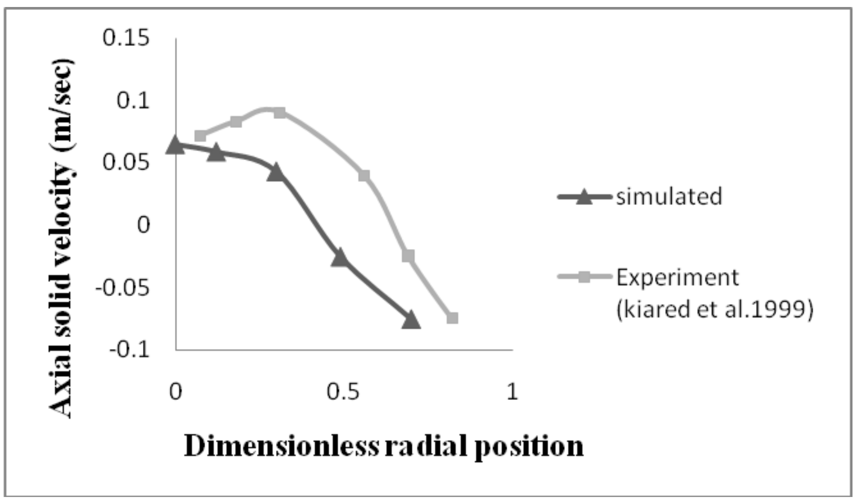

Fig. 5.10. Comparison of experimental work (Kiared et al., 1999) with simulation for axial solid velocity in 1.5 m height fluidized bed at [V_l = 0.065 m/s, V_g = 0.069 m/s, H_s = 0.35 m, D_p = 3 mm].

5.2.4. Axial velocity of solid, liquid and gas

The axial solid velocity at different bed height of solid with particle size 4.05 mm at the initial static bed height of 0.267 m along radial direction has been shown in Fig. 5.11. The velocity is found to decrease with bed height. It has been found that solid velocity has negative magnitude in some region which means that the solid is moving in both upward and downward direction in the fluidized bed. The lines at different bed height along radial direction have been created in 3D model for calculating the axial velocity profile. All these lines represent the axial velocity magnitude at respective bed height along radial direction. The axial solid velocity at bed height of 0.05 m found to be 0.005 m/s which decrease to 0.0025 m/sec at bed height of 0.1 m. The axial solid velocity profile has been found with negative magnitude at bed height 0.2 m. On small increase in bed height to 0.25 m, the negative magnitude increases. The axial velocity of solid becomes close to zero at bed height 0.3 m and above this the axial velocity magnitude is found to be zero.

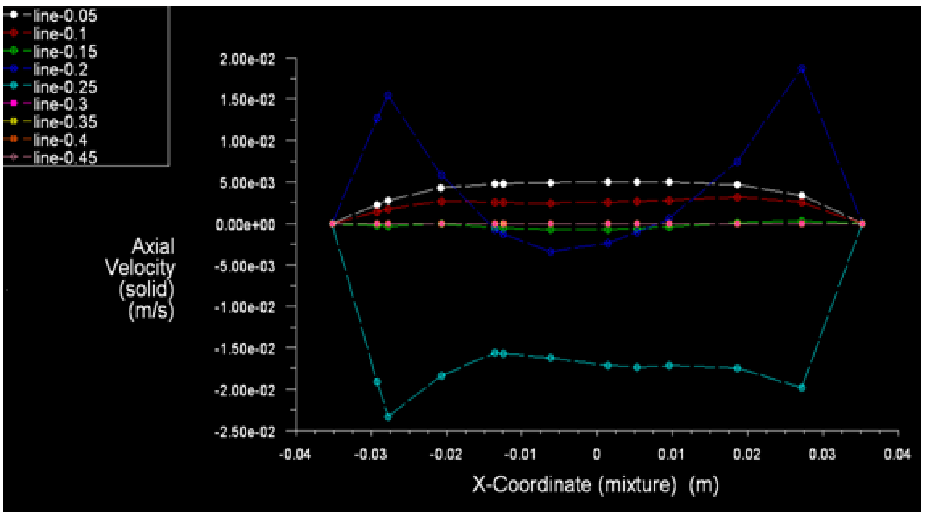

Fig. 5.11. Axial velocity of solid with radial direction in 1.88 m height fluidized bed at [V_l = 0.04 m/s, V_g = 0.02123 m/s, H_s = 0.267 m, D_p = 4.05 mm].

The axial velocity of liquid with initial static bed height 0.267 m along radial direction has been shown in Fig. 5.12. In axial velocity of liquid and gas profile the negative magnitude of velocity has not be seen.

The axial liquid velocity profile at the bed heights of 0.05 m, 0.1 m and 0.15 m varied nearly by a constant magnitude of 0.09 m/s. On increasing the bed height to 0.2 m, the axial liquid velocity profile starts to decrease and the magnitude near of 0.01 m/s at the bed height of 0.3 m has been found. On further increase in bed height the axial liquid velocity magnitude increases and becomes nearly constant magnitude of 0.03 m/s at bed heights of 0.35m, 0.4 m and 0.45 m.

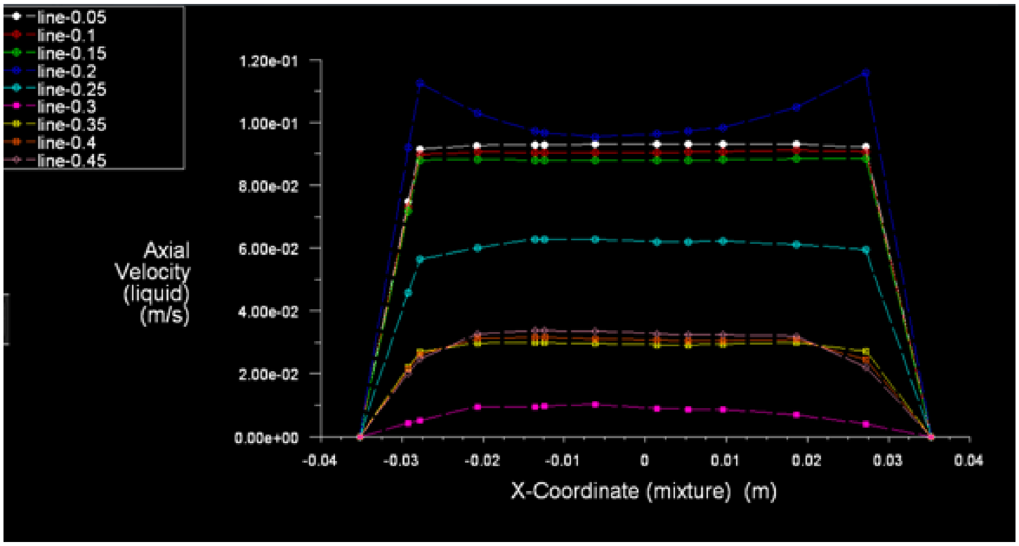

Fig. 5.12. Axial velocity of liquid with radial direction in 1.88 m height fluidized bed at [V_l = 0.04 m/s, V_g = 0.02123 m/s, H_s = 0.267 m, D_p = 4.05 mm].

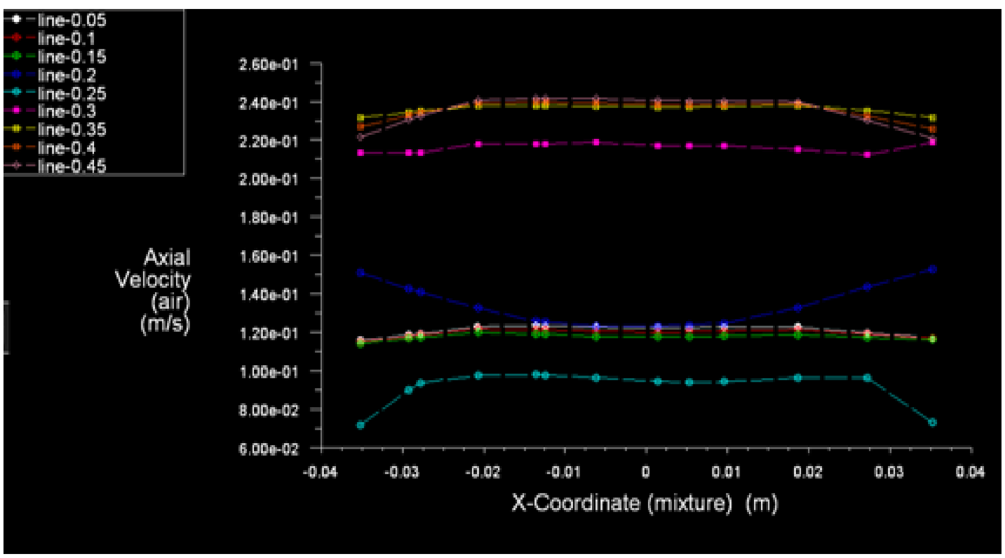

Fig. 5.13. Axial velocity of air with radial direction in 1.88 m height fluidized bed at [V_l = 0.04 m/s, V_g = 0.02123 m/s, H_s = 0.267 m, D_p = 4.05 mm].

The axial gas velocity profile at the bed heights of 0.05 m, 0.1 m and 0.15 m varied nearly by the constant magnitude of 0.12 m/s. as shown in Fig. 5.13. On increasing the bed height to 0.25 m, the axial gas velocity profile decreases with magnitude of nearly 0.093 m/s. On further increase in bed height the axial gas velocity magnitude increases and becomes nearly 0.21 m/s at the bed height of 0.3 m. The axial liquid velocity magnitude increases and becomes nearly constant in magnitude of 0.24 m/s at the bed heights of 0.35m, 0.4 m and 0.45 m.

5.2.5. Solid velocity of different particles with inlet liquid velocity

Fig. 5.14 shows the variation of magnitude of solid velocity of two different particles of diameter 2.18 and 4.05 mm varied with the same inlet liquid velocity at the constant gas velocity of 0.02123 m/s. The solid at the static condition in starting gains the velocity from liquid and gas. It has been observed that the smaller particle size gaining more velocity than the larger particles. The velocity difference between these two particles is more at low inlet velocity which become narrow when the inlet liquid velocity is high.

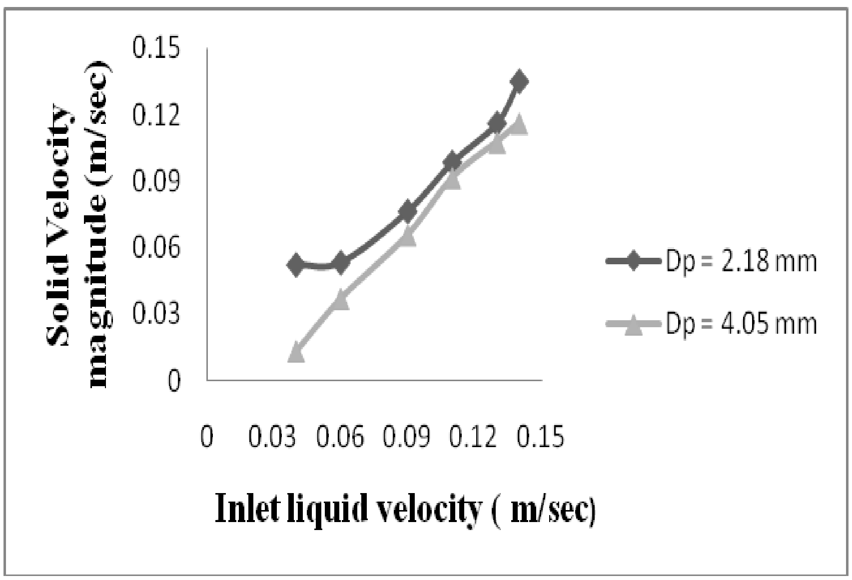

Fig. 5.14. Variation of solid velocity for different particles in 1.88 m height fluidized bed with the inlet liquid velocity at [V_g = 0.02123 m/s, H_s = 0.267 m].

5.2.6. Solid velocity comparison in different column

The profile of axial solid velocity with the radial direction for the initial solid static bed height of 0.267 m; column diameter of 0.1 m; particle size of 4.05mm; air inlet velocity of 0.02123 m/sec and water inlet velocity of 0.09 m/sec has been shown in Fig. 5.15. For column diameter 0.254 m with all other physical and operating condition kept same with 0.1m diameter column, the axial velocity profiles obtained has been shown in Fig. 5.16. The lines at different bed height along radial direction have been created in 3D model for calculating the axial solid velocity profile. All these lines represent the axial solid velocity magnitude at respective bed height along radial direction. The axial solid velocity magnitude profile in 0.1 m diameter column at 0.25 m bed height has been found to vary from -0.17 m/s to 0.15 m/s. On increasing the bed height further, the variation of axial solid velocity magnitude profile decreases along radial direction. In 0.254 m diameter column the axial solid velocity magnitude profile has been found with lower magnitude than 0.1 m diameter column. The velocity profile has been found more fluctuating along radial direction than the 0.1 m diameter column.

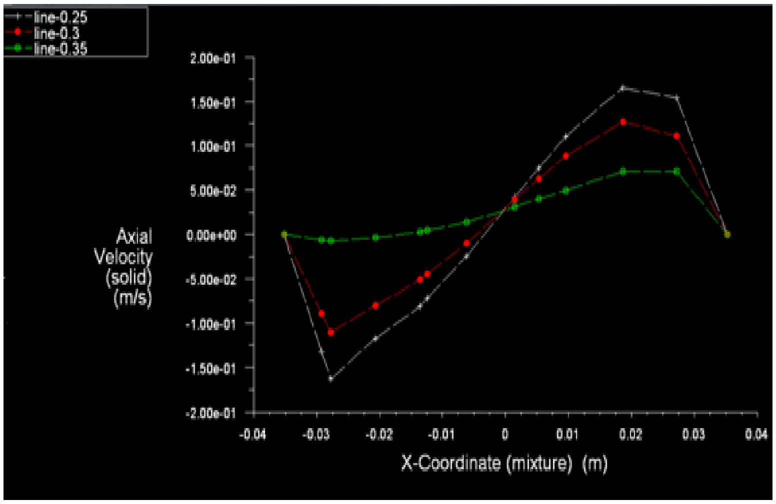

Fig. 5.15. Axial solid velocity profiles with radial direction for 0.1 m diameter fluidized bed at [V_l = 0.09 m/s, V_g = 0.02123 m/s, H_s = 0.267 m, D_p = 4.05 mm].

From the observation of both Fig. 5.15 and Fig. 5.16 it has been concluded that axial velocity in small diameter column is more than the large diameter column. The comparison of solid velocity magnitude with the bed height has been shown in Fig. 5.17 for the two different diameters of cylindrical column. The magnitude of average solid velocity and axial average solid velocity have been obtained by creating plane in 3D model up to required bed height along axial direction with taking the area weighted average value.

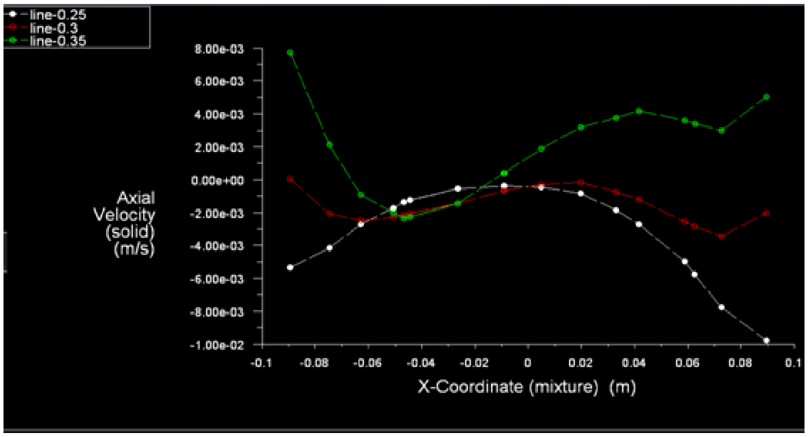

Fig. 5.16. Axial solid velocity profiles with radial direction for 0.254 m diameter column at [V_l = 0.09 m/s, V_g = 0.02123 m/s, H_s = 0.267 m, D_p = 4.05 mm].

.

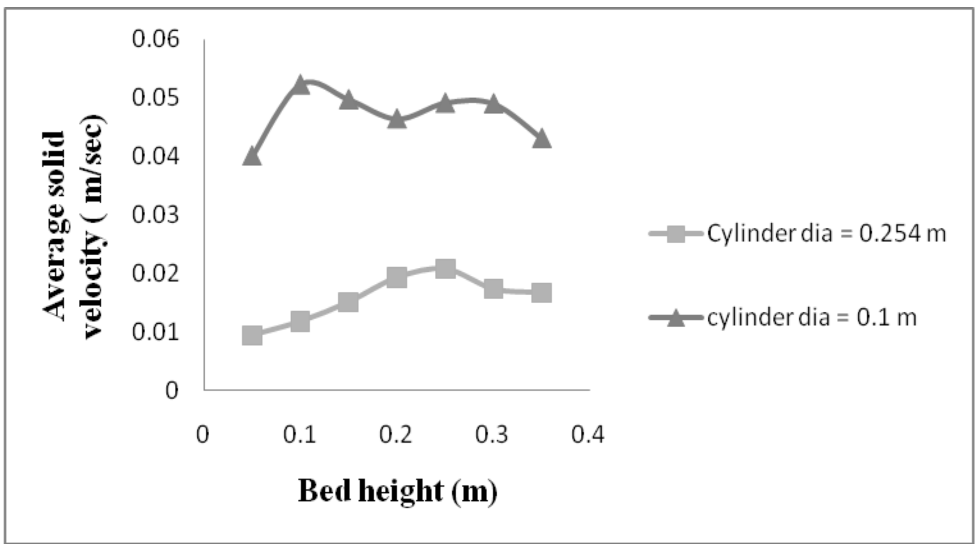

Fig. 5.17. Comparison of average solid velocity in two different cylinders with bed height at [V_l = 0.09 m/s, V_g = 0.02123 m/s, H_s = 0.267 m, D_p = 4.05 mm].

The axial solid velocity with bed height for different cylinders has been shown in Fig. 5.18. The axial solid velocity in small diameter column rises more at higher velocity than in the large diameter column. The axial solid velocity in larger column has been found to show small fluctuation.

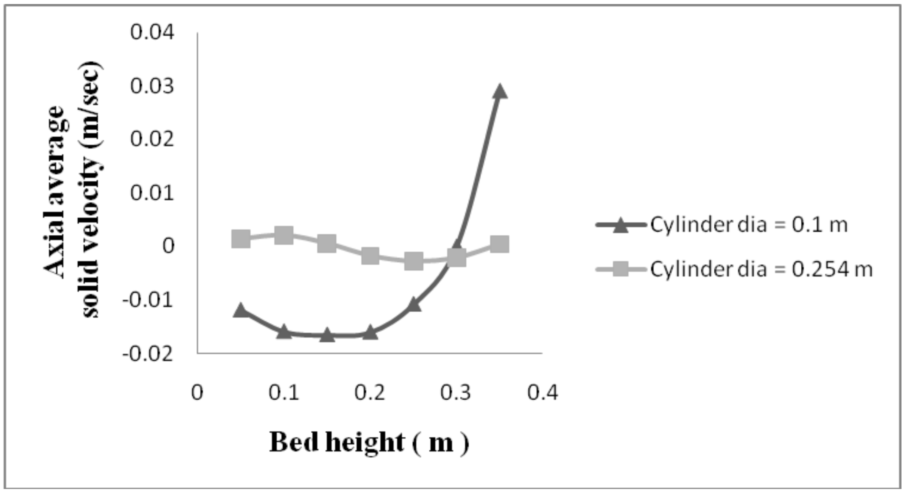

Fig. 5.18. Comparison of axial solid velocity in two different cylinders with bed height at [V_l = 0.09 m/s, V_g = 0.02123 m/s, H_s = 0.267 m, D_p = 4.05 mm].

5.2.7. Radial solid velocity

The radial solid velocity has been found to increase with the time for air inlet velocity of 0.02548 m/sec and water inlet velocity of 0.09 m/sec with 2.18 mm particle size as shown in Fig 5.19. At the time of 27 second the averaged radial velocity of solid found to be 0.06 m/s.

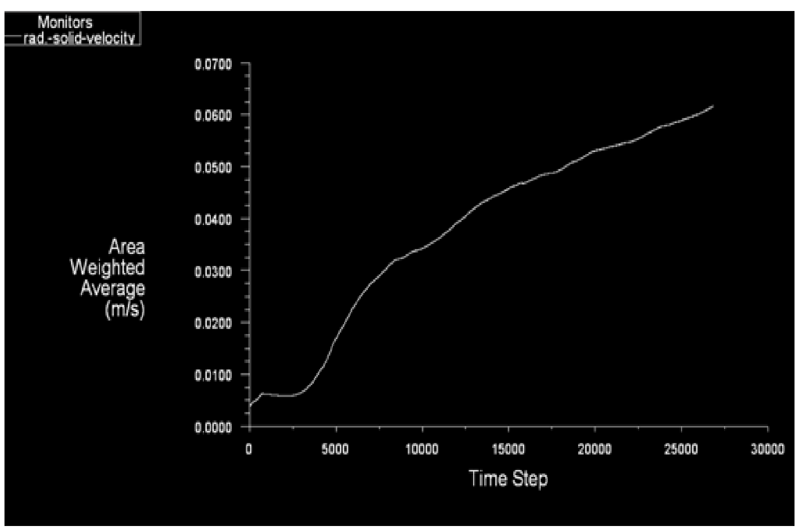

Fig. 5.19. Radial solid velocity variation with time step in 1.88 m height column at [V_l = 0.09 m/s, V_g = 0.02548 m/s, H_s = 0.213 m, D_p = 2.18 mm].

5.3 Bed Expansion

The bed expansion has been determined by taking X-Y plot of volume fraction of glass beads on Y-axis while height of the column at X-axis. From Fig. 5.20 the expended bed height of glass bead at liquid velocity of 0.0637 m/sec, gas velocity of 0.05096 m/sec and with initial bed height of 0.23 m has been found as 0.32 m.

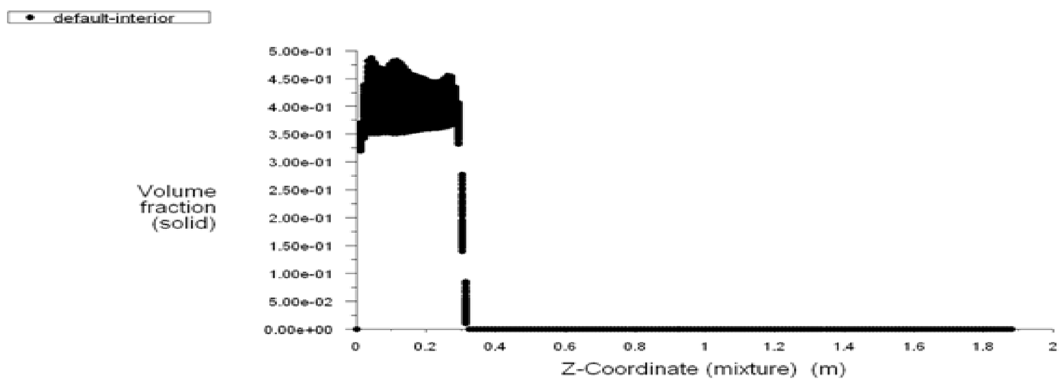

Fig. 5.20. Bed expansion of glass bead in 1.88 m height column at [V_l = 0.0637 m/s, V_g = 0.05096 m/s, H_s = 0.213 m, D_p = 2.18 mm].

Following are the trends of bed expansion vs. inlet water velocity shown in Fig. 5.21 obtained at different constant inlet air velocities, for initial bed height 21.3cm and particle size 2.18mm which shows that the bed expands when water velocity increases.

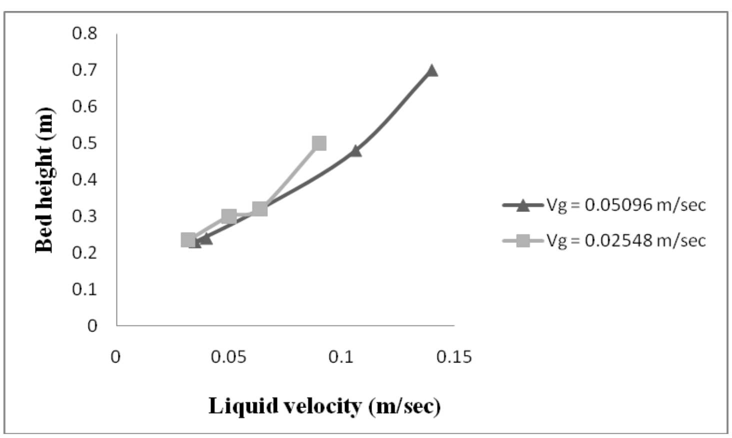

Fig. 5.21. Bed height variation with inlet liquid velocity at constant gas inlet velocity for 1.88 m height fluidized bed at [H_s = 0.213 m, D_p = 2.18 mm].

The bed expansion depends on the size of particles. The bed expansion ratio of two different particle size of glass bead 2.18mm and 4.05 mm with different inlet liquid velocity and constant inlet air velocity at the same initial static bed height of 0.267 m has been shown in Fig. 5.22. This result obtained from CFD simulation has been compared with experimental result of Jena (2009), which shows good agreement with small deviation.

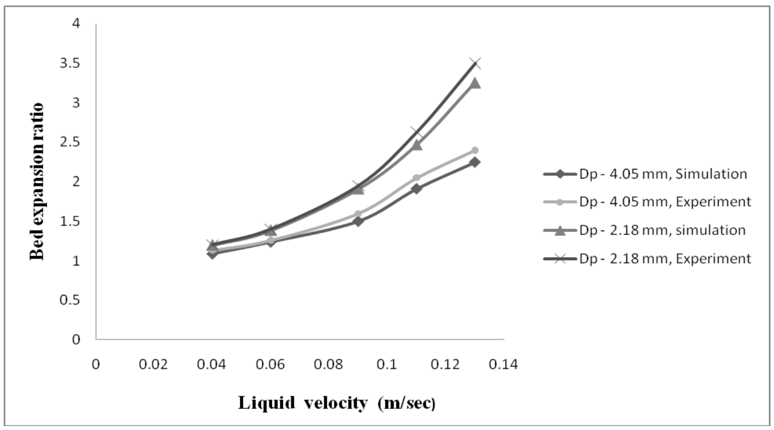

Fig. 5.22. Comparison of bed expansion ratio of two different glass beads with experiment in 1.88 m height column at [V_g = 0.02123 m/s, H_s = 0.267 m].

The reason for small deviation may be that the glass beads used in experiment have a range of diameters while in the simulation all glass beads are taken to be of the same diameter. The bed height with 2.18 mm glass beads has been found more than the 4.05 mm glass bead, also with increasing the liquid velocity the bed height has also been found to increase.

5.4. Gas hold up

Gas holdup has been obtained as by creating plane in 3D model up to required bed height along axial direction with taking the area weighted average volume fraction of air in the fluidized region of the column. Fig 5.23 shows the variation of gas hold up with inlet liquid velocity for 4.05 mm particles with 0.267 m of static bed height. The gas hold up has been found to decrease with the increasing of inlet liquid velocity.

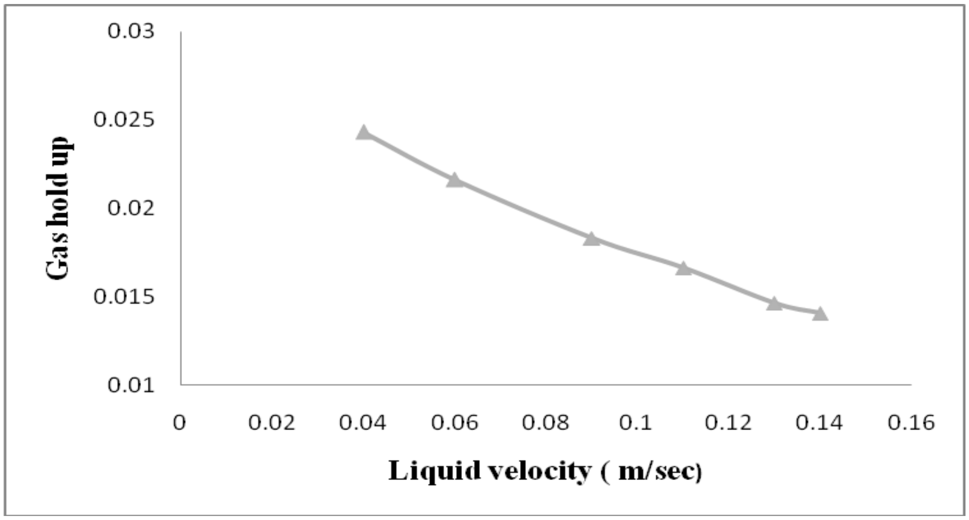

Fig. 5.23. Gas hold up variation with inlet liquid velocity for 1.88 m height column at [V_g = 0.02123 m/s, H_s = 0.267 m, D_p = 4.05 mm].

5.5. Bed voidage

The bed voidage or bed porosity is defined as the fraction of the bed volume occupied by both liquid and gas phases. Fig. 5.24 shows the bed voidage variations of two different particles size with the inlet liquid velocity. Bed voidage is a strong function of liquid velocity; it increases with the liquid velocity. The small the particle size has more bed voidage than the larger particle size.

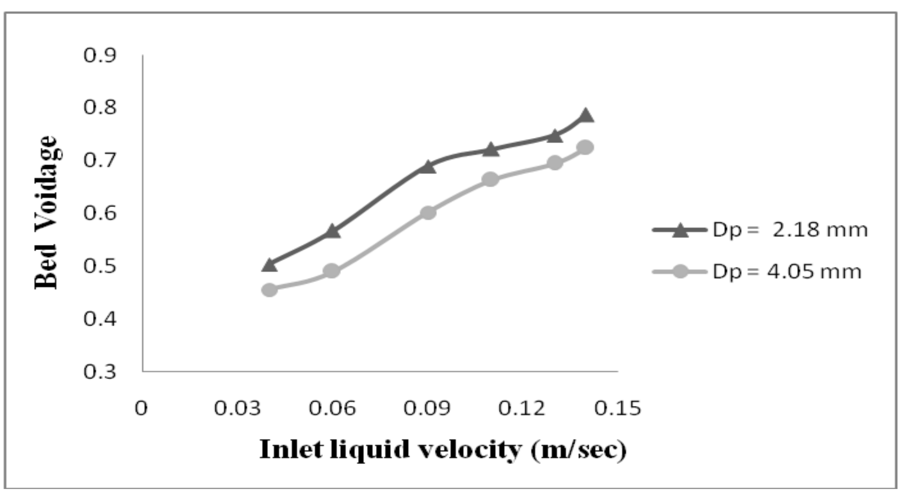

Fig. 5.24. Comparison of bed voidage of different particles in 1.88 m height column with the inlet liquid velocity at [V_g = 0.02123 m/s, H_s = 0.267 m].

The bed voidage in the fluidized bed increases with the velocity of solid If the particles are static the bed voidage is found to be minimum, it starts to increase with the velocity of solids. Fig. 5.25 shows the extent of increasing bed voidage with the magnitude of solid velocity in the fluidized bed for 4.05 mm particle.

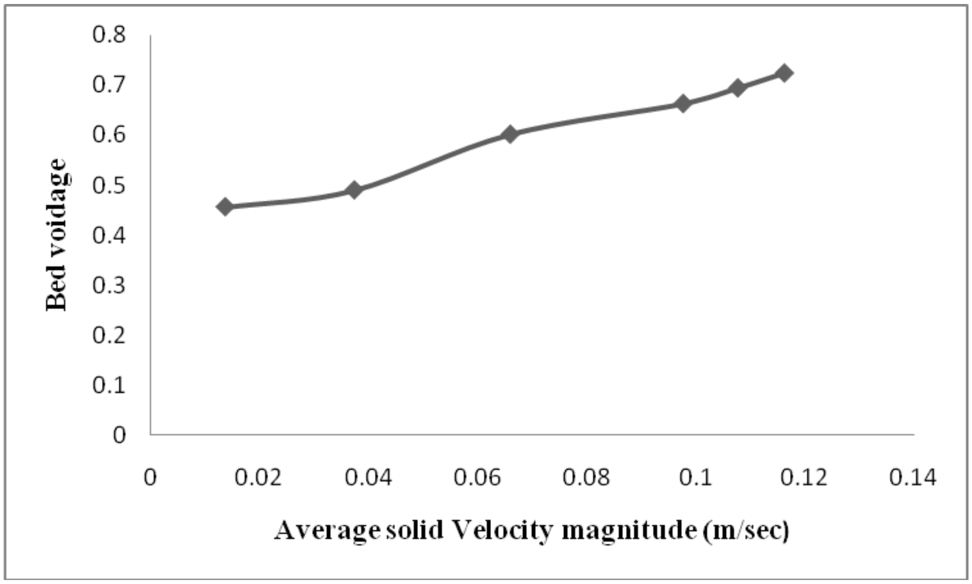

Fig. 5.25. Bed voidage variation with solid velocity for 4.05 mm particle in 1.88 m height column with the inlet liquid velocity at [V_g = 0.02123 m/s, H_s = 0.267 m, D_p = 4.05 mm].

5.6. Liquid hold up

Fig. 5.26 shows the variation of liquid holdup with inlet liquid velocity at constant gas velocity of two different particle size glass beads. It has been observed that with the increase in liquid velocity the liquid holdup increases sharply It has been seen that with increase in particle size the liquid holdup decreases.

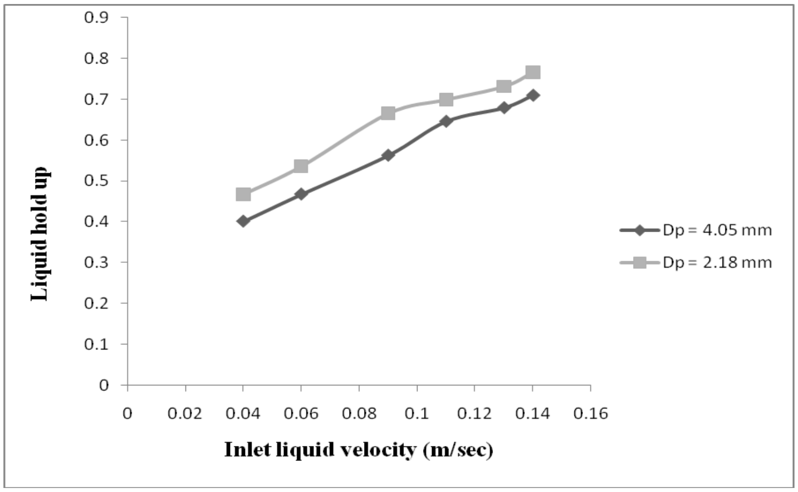

Fig. 5.26. Liquid hold up variation with inlet liquid velocity for different particles in 1.88 m height column at [V_g = 0.02123 m/s, H_s = 0.267 m].

The liquid hold up variation has been compared with experimental data of Jena (2009) as shown in Fig. 5.27. The simulated results have been found good agreement with experiment.

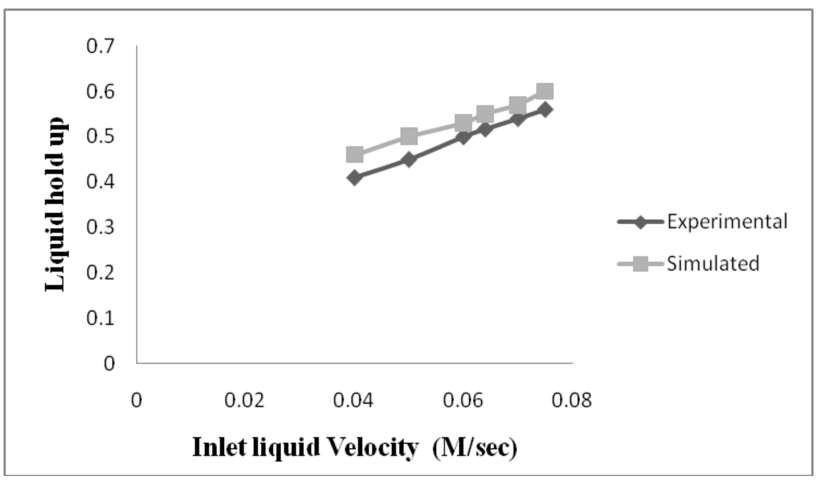

Fig. 5.27. Comparison of liquid hold up simulation profiles with experiment for 1.88 m height column at [V_g = 0.02123 m/s, H_s = 0.267 m, D_p = 2.18 mm].

The liquid hold up simulated results have been plotted with experimental results and there is nearly straight line variation have been found as shown in Fig. 5.28.The average percentage deviation of simulated results with experimental have been found as 7.4 %.

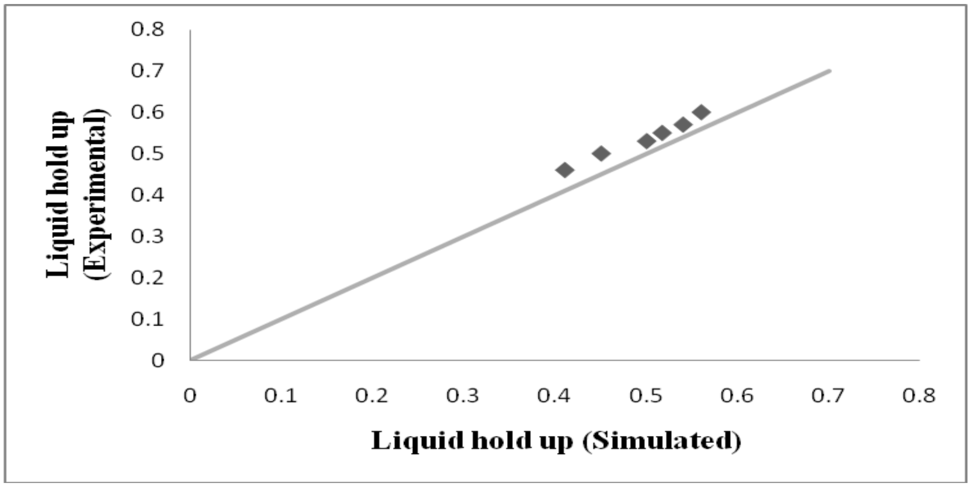

Fig. 5.28. Liquid hold up (experimental vs. simulated results) for 1.88 m height column at [V_g = 0.02123 m/s, H_s = 0.267 m, D_p = 2.18 mm].

5.7. Pressure drop

The Contours plot of static gauge pressure (mixture phase) in the column obtained at water velocity of 0.06 m/s and air velocity of 0.01 m/s. of 2.5 m height of cylindrical column are shown in Fig. 5.29.

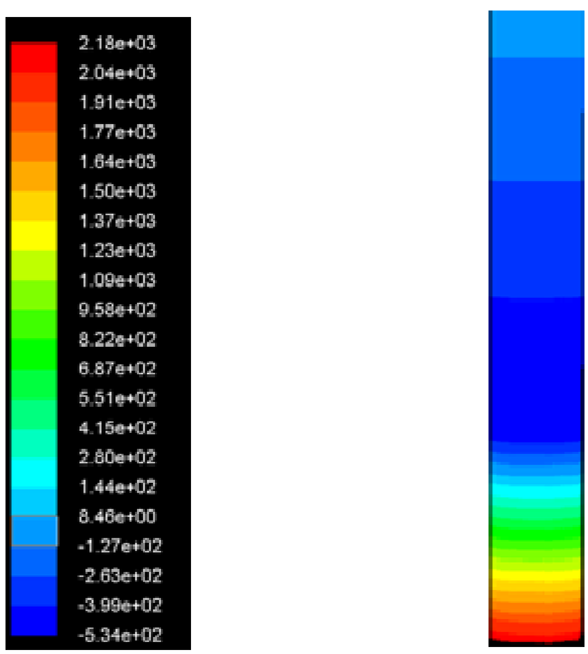

..

Fig. 5.29. Contours of static gauge pressure (mixture phase) in 2.5 m height column at [V_l = 0.06 m/s, V_g = 0.01 m/s, H_s = 0.39 m, D_p =2 3 mm].

This contour illustrates that pressure increases as we move from top to bottom. Pressure at inlet and outlet can also be determined which is helpful in finding the pressure drop across bed.

5.8 Frictional pressure drop at wall

The frictional pressure drop at the wall with incresing in bed height at different gas and liquid velocity of glass beads 2.18 mm at the static bed height of 0.213 m are shown in Fig. 5.30. The trends of frictional pressure drop at the wall with varying water velocity at constant air velocity at with glass beads of size 4.05 mm at initial static bed height of 0.267 m are shown in Fig. 5.31.The frictional pressure drop has been obtained by using area weighted average value of shear stress at wall. On incresing in the bed height the frictional pressure drop has been found to decrease.

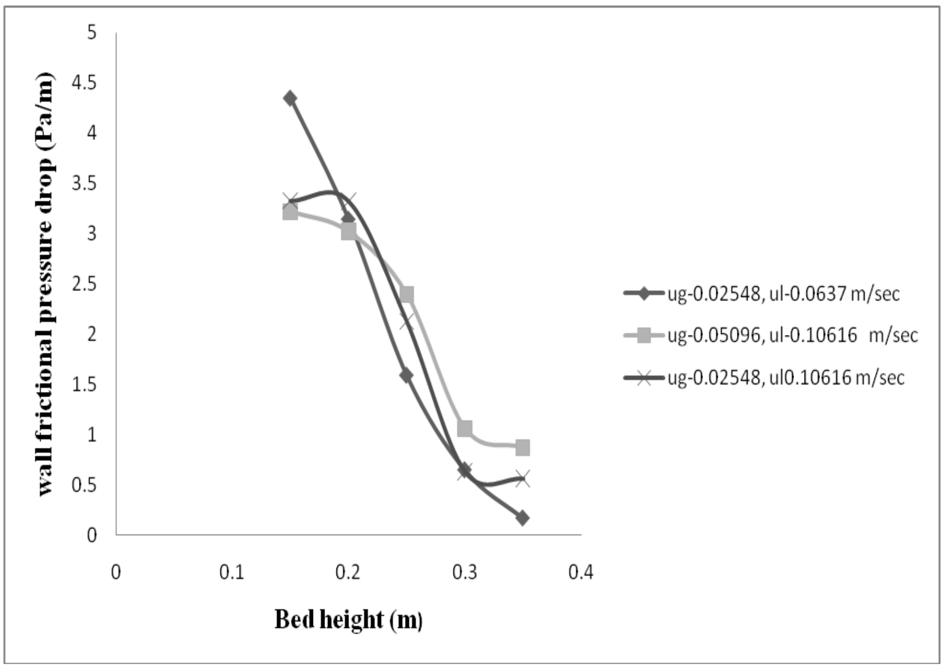

Fig. 5.30. Wall frictional pressure drop with bed height in 1.88 m height column for different gas and liquid velocity at [H_s = 0.213 m, D_p = 2.18 mm].

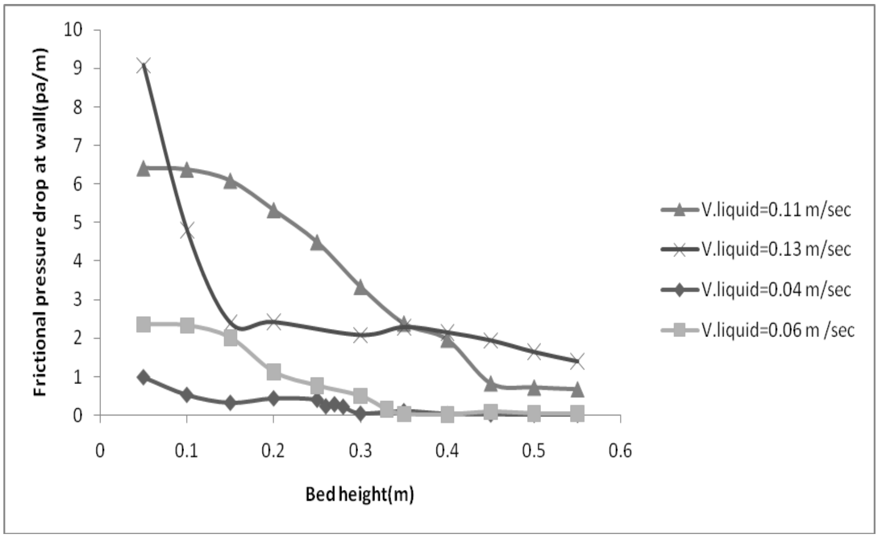

Fig. 5.31. Wall frictional pressure drop with bed in 1.88 m height column at [V_g = 0.02123 m/s, H_s = 0.267 m, D_p = 4.05 mm].

5.9. Turbulence kinetic energy

Turbulence kinetic energy (TKE) is the mean kinetic energy per unit mass associated with eddies in turbulent flow. Turbulence kinetic energy with flow time for 1.88 m height column variation has been shown in Fig.5.32. Turbulent kinetic energy is generated from fluctuation in velocity.

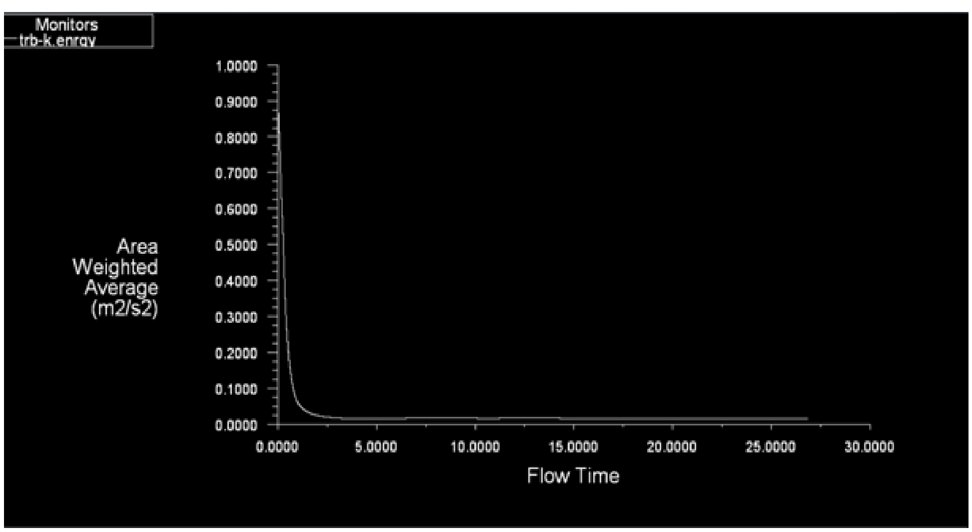

Fig. 5.32. Turbulence kinetic energy with flow time for 1.88 m height column at [V_l = 0.09 m/sec, V_g = 0.02548 m/s, H_s = 0.213 m, D_p = 2.13 mm].

Physically, the turbulence kinetic energy is characterized by measured root-mean-square (RMS) velocity fluctuations. Turbulence kinetic energy is produced by fluid shear, friction and buoyancy. The turbulence kinetic energy has been observed decreasing with the time for air inlet velocity of 0.02548 m/sec and water inlet velocity of 0.09 m/sec with 2.18 mm particle size and finally it becomes constant with the time in fluidization.

5.10. Computation of various energy flows

In gas–liquid–solid fluidized beds, the input energy from the gas and liquid is distributed to the mean flow of the liquid, gas, and the solid phases. Also, a part of the input energy is used for liquid phase turbulence and some part of the energy gets dissipated due to the friction between the liquid and solid phases and the gas and liquid phases. The energy entering in the system increases with liquid velocity. The computation of various energy flows and net energy differences are tabulated in table 5.1.

Table 5.1 Energy flow calculations for 1.88m height column with initial bed height 21.3 cm

Liquid velocity (m/sec)	Gas velocity (m/sec)	Energy inlet (W)	Energy Out(W)	E_t (W)	E_e (W)	E_{bls}(W)	(E_{bgl} (W)	Energy difference (W)
0.0637	0.02548	3.727087	1.520477	0.177728	0.02381	0.007982	0.648411	1.34868
0.10616	0.02548	8.339432	3.76153	1.142763	0.0495	0.005271	0.61751	2.762858
0.0637	0.05096	4.763128	1.570262	0.441574	0.02499	0.010083	0.980623	1.735597
0.10616	0.05096	10.07573	3.926026	0.616645	0.0584	0.02105	1.174703	4.278911

Where, Et Energy gained by solid.

E_e Energy dissipation rate due to turbulence in liquid phase by liquid phase turbulence.

(E_{bls}) Energy dissipation rate due to friction at liquid solid interphase.

(E_{bgl}) Energy dissipation rate due to friction at gas -liquid interphase.

Chapter 6

Conclusion & Future Scope of The Work

Chapter–6

Conclusion and future scope of the work

6.1. Conclusion

CFD simulation of hydrodynamics of three phase fluidized bed has been carried out for different operating and physical condition by employing the Eulerian - Eularian approach. Three-dimensional numerical simulations of fluidized bed column have been carried out for different configurations. In three phase fluidization the hydrodynamics variables studied include gas, liquid and solid hold up, bed expansion, bed voidage, velocity distribution profiles of all phases, pressure drop, frictional pressure drop at wall, energy flows, and operating variables varied include liquid and air velocity, initial static bed height and particle size. The interactions between the gas, solids, and liquid that are difficult to investigate in experiments have been studied numerically. The main conclusions which have been pointed out are as follows:

- The velocity magnitude of all phases found to increase initially, maximum at 0.1 m bed height and then the magnitude decreases with the bed height for glass beads of 2.18 mm. Solid velocity found to be zero above the bed height where as gas and liquid velocity becomes constant above the bed height with nearly small range velocity.
- The magnitude of velocity of all phases has been found to be more at the center region than near the wall.
- The velocity profiles of both liquid and solid in fluidized bed have been increasing with time in starting and then it goes on to decrease showing the oscillatory behavior with decreasing amplitude. It means that for a given initial condition the velocity will reach maximum only once after starting the fluidization.
- The parabolic path has been observed for liquid velocity in fluidized bed along radial direction.
- In comparison with each other phases in cylindrical column, the velocity of gas phase has been found maximum in the column.
- The smaller particles gain more velocity than the larger particles for same condition in fluidized bed.

- Axial solid velocity in small diameter column has been found to be more than in the large diameter column.
- The expanded bed height is strong function of liquid velocity. The bed expansion ratio increases with liquid velocity at constant gas velocity and depends strongly on particle size. For larger particle size bed expansion ratio has been found to be lower than the larger particle size.
- Gas hold up decreases with increase in liquid inlet velocity.
- Bed voidage increases with the liquid inlet velocity and small particle size has more bed voidage than the larger particle size.
- On increasing liquid velocity the liquid hold up increases sharply. Liquid holdup is found to be low for large particle size as compared with the small size particles under identical conditions.
- The static pressure decreases with increase in the bed height.
- On incresing the bed height the frictional pressure drop at wall has been found to be decreased. Frictional pressure drop is a strong function of liquid velocity, for high liquid velocity the preesure drop has been found to be more.
- The energy entering in the system increases more with liquid velocity and the net energy difference which should account for energy dissipated in system increases with both gas and liquid velocity.
- The axial velocity of solid along radial coordinate for 1.5 m height column has been validated with the experimental work. The bed expansion ratio and liquid hold up for different particle size has also been found to be at good agreement with experimental work.

6.2. Future scope of the work

The Eulerian-Eulerian multi-phase granular flow approach is capable of predicting the overall performance of a gas–liquid–solid fluidized bed. This model can be used to verify more experimental work in future. The present simulation has been done for small scale system although the conclusions from this small-scale system may be also applicable to large industrial scale plant for scale-up study. It may be applied for various other investigations and troubleshooting in industries.

References

- Allia, K., Tahar, N., Toumi, L., Salem, Z., 2006. Biological treatment of water contaminated by hydrocarbons in three-phase gas-liquid-solid fluidized bed Global Nest. The Chemical Engineering Journal 8, 9–15.
- Anderson, J. D., 1995. Computational fluid dynamics. McGraw Hill, New York.
- Bahary, M., 1994. Experimental and computational studies of hydrodynamics in three-phase and two-phase fluidized beds. Ph.D. thesis. Illinois Institute of Technology, Chicago.
- Bakker, A., 2002. Fluent introductory notes. Fluent Inc, Lebanon.
- Comte,M. P., Bastoul, D., Hebrard, G., Roustan, M., Lazarova, V., 1997. Hydrodynamics of a three-phase fluidized bed - the inverse turbulent bed. Chemical Engineering Science 52, 3971– 3977.
- Dudukovic, M. P., Larachi, F., Mills, P. L., 1999. Multiphase reactors-revisited Chemical Engineering Science 54, 1975–1995.
- Epstein, N., 1981. Three-Phase Fluidization: Some knowledge gaps. Can.J.Chem.Engg 59, 649-757.
- Fan, L.S., Muroyama, K., Chern, S.H., 1982. Hydrodynamic characteristics of inverse fluidization in liquid–solid and gas–liquid–solid systems. The Chemical Engineering Journal 24, 143-150.
- Feng, W., Wen, J., Fan, J., Yuan, Q., Jia, X., Sun, Y., 2005. Local hydrodynamics of gas–liquid–nano particles three-phase fluidization. Chemical Engineering Science 60, 6887–6898.
- Ferziger, J.H., Peric, M., 2002. Computational method for fluid dynamics. Third edition, Springer, New York.
- Fluent 6.2 Documentation., 2005. Lebanon, Fluent Inc.
- Gamwo, I. K., Lyczkowski, R. W., Soong, Y., 1998. Numerical simulation and experimental validation of solids flows in a bubbling fluidized bed Powder Technol 103. 1703–1713.

- Grevskott, S., Sannaes, B. H., Dudukovic, M. P., Hjarbo, K. W., Svendsen, H. F., 1996. Liquid circulation bubble size distributions and solids movement in two-and three-phase bubble columns. Chemical Engineering Science 51, 1703–1713.
- Howard, J. R., 1989. Fluidized Bed Technology: Principles and Applications. Adam Higler, New York.
- Jena, H. M., Roy, G. K., Meikap, B. C., 2009. Hydrodynamics of a gas-liquid-solid fluidized bed with hollow cylindrical particles. Chemical Engineering and Processing, Process Intensification 48, 279-287.
- Jena, H. M., 2009. Hydrodynamics of Gas-Liquid-Solid Fluidized and Semi-Fluidized Beds., Ph.D thesis. National institute of technology, Rourkela.
- Jianping, W., Shonglin, X., 1998. Local hydrodynamics in a gas–liquid–solid three phase bubble column reactor. Chemical Engineering Journal 70, 81–84.
- Joshi. J. B., 2001. Computational flow modeling and design of bubble column reactors. Chemical Engineering Science 56**,** 5893–5933.
- Joshi J. B., Vitankar, V. S., Dhotre, M. T., 2002. A low Reynolds number k–ε model for the prediction of flow pattern and pressure drop in bubble column reactors. Chemical Engineering Science 57, 3235 – 3250.
- Kiared, K., Larachi, F., Chaouki, J., Guy, C., 1999. Mean and turbulent particle velocity in the fully developed region of a three-phase fluidized bed. Chemical Engineering & Technology. 22**,** 683–689.
- Krishnaiah, K., Guru, S., Sekar, V., 1993. Hydrodynamic studies on inverse gas-liquid-solid fluidization. The Chemical Engineering Journal 51, 109 – 112.
- Kunii, D., Levenspiel, O., 1991. Fluidization Engineering. 2nd edition, Butterworth-Heinemann, Washington.
- Li, Y., Zhang, J., Fan, L. S., 1999. Numerical simulation of gas–liquid–solid fluidization systems using a combined CFD–VOF–DPM method, bubble wake behavior. Chemical Engineering Science 54, 5101–5107.
- Matonis, D., Gidaspow, D., Bahary, M., 2002. CFD simulation of flow and turbulence in a slurry bubble column. A.I.Ch.E. Journal 48, 1413–1429.

- Mitra-Majumdar, D., Farouk, B., Shah, Y. T., 1997. Hydrodynamic modeling of three-phase flows through a vertical column. The Chemical Engineering Science 52, 4485 – 4497.
- Muroyama, K., Fan, L. S., 1985. Fundamentals of gas-liquid-solid fluidization. A.I.Ch.E. Jounral 31, 1-34.
- Muthu, M. K., Natarajan, E., 2008. CFD simulation for two-phase mixing in 2D fluidized bed. The International Journal of Advanced Manufacturing Technology.
- O'Rourke, P. J., Zhao, P. P., Snider, D., 2009. A model for collisional exchange in gas-liquid-solid fluidized beds. The Chemical Engineering Science 64, 1784-1797.
- Park, H., 2009. CFD Advantages and Practical Applications Glumac Inc.
- Padial, N. T., Van der Heyden, W. B., Rauenzahn, R. M., Yarbro, S. L., 2000. Three dimensional simulation of a three-phase draft-tube bubble column. Chemical Engineering Science 55, 3261–3273.
- Pain C. C., Mansoorzadeh, S., de Oliveira, C. R. E., 2001. A study of bubbling and slugging fluidised beds using the two-fluid granular temperature model. International Jounral Multiphase Flow 27, 527–551.
- Panneerselvam, R., Savithri, S., Surender, G. D., 2009. CFD simulation of hydrodynamics of gas–liquid–solid fluidized bed reactor. Chemical Engineering Science 64, 1119-1135.
- Schallenberg, J., Enb, J. H., Hempel, D. C., 2005. The important role of local dispersed phase hold-ups for the calculation of three-phase bubble columns. Chemical Engineering Science 60, 6027–603.
- Sokol, W., Halfani, M. R., 1999. Hydrodynamics of gas-liquid-solid fluidized bed bioreactor with a low density biomass support. Biochem Eng Journal 3, 185 – 192.
- Trambouze, P., Euzen, J., 2004. Chemical Reactors, From Design to Operation. Technip, Paris.
- Wen, Y.,Soung., 1978. Bed Expansion in Three-Phase Fluidization Industry Engineering. Chemical Process Des. Dev. 17, 33–36.

- Zhang, X., Ahmadi, G., 2005. Eulerian–Lagrangian simulations of liquid–gas–solid flows in three-phase slurry reactors. Chemical Engineering Science 60, 5089– 5104.

Curriculum Vitae

SHAILENDRA KUMAR PANDEY

EMAIL ID	:	skpandeychem24@gmail.com
PHONE	:	09692568069
Permanent Address	:	145-B/12I Govindpur, Allahabad U.P - 211004
Date of Birth	:	30-AUGUST- 1985

EDUCATIONAL QUALIFICATION

- **M.Tech** in **Chemical Engineering (**Thesis submitted) from NATIONAL INSTITUTE OF TECHNOLOGY ROURKELA in 2010.
- **B.Tech in Chemical Engineering** from I.E.T M.J.P ROHILKHAND UNIVERSITY BAREILLY (U.P) with **7.58** Grade point marks in 2008.
- **HIGH SCHOOL** Passed in year 2000 from kendriya Vidyalaya Old Cantt. Allahabad. (CBSE Board) with 72% marks.
- **INTERMEDIATE** Passed in year 2002 from kendriya Vidyalaya Old Cantt. Allahabad. (CBSE Board) with 58% marks.

Conference

Shailendra kumar pandey and Abanti sahoo**, "Studies on drying efficiency & shrinkage of different shaped food particles in a fluidized bed dryer: Emperical models". 62nd annual session, Indian institute of Chemical engineers, (CHEMCON - 2009), 27- 30 Dec 2009. Andhra university, Vishakhapatnam.**